# Crosstalk between repair pathways elicits double-strand breaks in alkylated DNA and implications for the action of temozolomide

Robert P Fuchs, Asako Isogawa, Joao A Paulo, Kazumitsu Onizuka, Tatsuro Takahashi, Ravindra Amunugama, Julien Duxin, Shingo Fujii

Title:

# Crosstalk between repair pathways elicits Double-Strand Breaks in alkylated DNA: implications for the action of temozolomide.

Key words: alkylating agents / SN1 versus SN2 /*O*-alkylation versus N-alkylation/ unbiased discovery of DNA Binding proteins/ IDAP/ temozolomide / Mismatch Repair and Base Excision Repair crosstalk / protein-DNA pull-down assay / Mass Spectrometry protein identification / neighboring lesions / double-strand breaks

Authors:
Robert P. Fuchs[a,1,2], Asako Isogawa[b], Joao A. Paulo[c], Kazumitsu Onizuka[d], Tatsuro Takahashi[e], Ravindra Amunugama[a], Julien Duxin[a,3] and Shingo Fujii[b].

a: Department of Biological Chemistry and Molecular Pharmacology, Harvard Medical School, Boston, MA 02115 (USA).
b: Cancer Research Center of Marseille, UMR7258, CNRS, INSERM, AMU Marseille, France
c: Department of Cell Biology, Harvard Medical School, Boston, Massachusetts 02115, USA
d: Institute of Multidisciplinary Research for Advanced Materials, Tohoku University, Sendai, Miyagi 980-8577, Japan.
e: Faculty of Science, Kyushu University, 744 Motooka, Nishi-ku, Fukuoka 819-0395, Japan

1: present address: Marseille Medical Genetics, UMR1251, AMU and INSERM Marseille, France
2: to whom correspondence should be addressed: robert.fuchs@inserm.fr
3: present address: The Novo Nordisk Foundation Center for Protein Research, University of Copenhagen, Copenhagen, Denmark

Until now, the cytotoxic effect of SN1 alkylating agents was attributed to MMR acting on $O^6$mG:T lesions that form following replication. Our paper highlights that $O^6$mG:C lesion *per se* is a MMR target that can trigger DSB through coupling with BER.

Abstract:
Temozolomide (TMZ), a DNA methylating agent, is the primary chemotherapeutic drug used in glioblastoma treatment. TMZ induces mostly N-alkylation adducts (N7-methylguanine and N3-methyladenine) and some $O^6$-methylguanine ($O^6$mG). Current models propose that during DNA replication, thymine is incorporated across from $O^6$mG, promoting a futile cycle of mismatch repair (MMR) that leads to DNA double strand breaks (DSBs). To revisit the mechanism of $O^6$mG processing, we reacted plasmid DNA with N-Methyl-N-nitrosourea (MNU), a temozolomide mimic, and incubated it in Xenopus egg-derived extracts. We show that in this system, mismatch repair (MMR) proteins are enriched on MNU-treated DNA and we observe robust, MMR-dependent, repair synthesis. Our evidence also suggests that MMR, initiated at $O^6$mG:C sites, is strongly stimulated in *cis* by repair processing of other lesions, such as N-alkylation adducts. Importantly, MNU-treated plasmids display DSBs in extracts, the frequency of which increased linearly with the square of alkylation dose. We suggest that DSBs result from two independent repair processes, one involving MMR at $O^6$mG:C sites and the other involving BER acting at a nearby N-alkylation adducts. We propose a new, replication-independent mechanism of action of TMZ, that operates in addition to the well-studied cell cycle dependent mode of action.

## Introduction:

Alkylating agents, a class of important environmental carcinogens, have been widely used in molecular biology to study fundamental repair processes and in the clinic to treat cancer patients. Among the DNA adducts produced by methylating agents such as N-methyl-N-nitrosourea (MNU) and temozolomide (TMZ), a clinically used mimic, the most abundant are two N-alkylation adducts, at the N7 position of guanine (7mG: 70-75% of total alkyl adducts) and the N3 position of adenine (3mA: 8-12%). Importantly, both reagents also produce 8-9% O-alkylation adducts in the form of $O^6$-methylguanine ($O^6$mG). This feature contrasts with another common methylating agent, methyl-methane sulfonate (MMS), which forms a much lower level of $O^6$mG (<0.3%) while producing similarly high proportions of 7mG (81-83%) and 3mA (10-11%)(Beranek, 1990). For many years, the differences in O versus N reactivities have been rationalized by differences in chemical reaction mechanisms; on one side, compounds such as MMS, with very low O-reactivity were classified as an SN2 agent (bimolecular nucleophilic substitution) while other agents, such as MNU and TMZ, with increased O adduct formation were called SN1 agents (monomolecular nucleophilic substitution). While this classification turned out not to be mechanistically accurate (Loechler, 1994), we will nevertheless use this nomenclature throughout this paper for the sake of simplicity. The major N-alkylation (N-alkyl) adducts (7mG and 3mA) are repaired by base excision repair (BER), using N-methylpurine-DNA glycosylase (MPG) also known as 3-alkyladenine DNA glycosylase (AAG) and alkylpurine DNA N-glycosylase (APNG) (Chakravarti et al., 1991; Lindahl, 1976). O-alkylation adducts ($O^6$mG, $O^4$mT) can be directly repaired by $O^6$-methylguanine-DNA methyl transferase (MGMT), a protein that transfers the methyl group from these adducts to one of its cysteine residues (Demple et al., 1982; Olsson and Lindahl, 1980; Tano et al., 1990). In addition, alkylating agents also produce a variety of other minor (1-2%) N-alkyl adducts, namely 1mA, 3mC, 3mT and 1mG that are directly demethylated by AlkB homologs (Aas et al., 2003; Duncan et al., 2002; Falnes et al., 2002; Trewick et al., 2002).

In summary, SN1 and SN2 alkylating agents produce a diverse array of DNA adducts, but they differ greatly in the amount of $O^6$mG produced.

Agents such as MMS mostly induce N-alkyl adducts that lead to DSBs during S-phase as a consequence of BER repair. Indeed, inactivation of the AAG glycosylase, the BER initiating enzyme, suppresses DSB while inactivation of Pol β leads to their exacerbation (Simonelli et al., 2017; Tang et al., 2011; Trivedi et al., 2005). In rodent cells, it was proposed that MMS-induced DSBs arise when replication meets BER-induced single-strand breaks (Ensminger et al., 2014). The toxicity of N-alkyl adducts was found to depend on the cell type. AAG-mediated repair of N-alkyl adducts was found to mitigate toxicity in mouse ES cells and HeLa cells, while repair was shown to cause toxic intermediates in retina and bone marrow cells (Meira et al., 2009). In all cell type, *O*-alkyl adducts were found to be highly cytotoxic and mutagenic. While the mutagenicity of $O^6$mG is easily accounted for by its high propensity to mispair with T during DNA synthesis (Bhanot and Ray, 1986; Loechler et al., 1984; Mazon et al., 2010) its cytotoxicity is intriguing since $O^6$mG *per se* does not interfere with DNA synthesis. A seminal paper, published 50 years ago by Plant and Roberts (Plant and Roberts, 1971), noted that when synchronized HeLa cells are treated in G1 with MNU, they continue through the first cell cycle almost normally and with little effect on DNA synthesis. On the other hand, there is a dramatic effect on DNA synthesis in the second cell cycle after MNU exposure. These data led the authors to surmise that cytotoxicity stems from a secondary lesion that forms when DNA synthesis occurs across $O^6$mG template adducts (Plant and Roberts, 1971). It was demonstrated later that MNU-mediated inhibition of DNA synthesis, in the first and second cycle, is due to the action of the mismatch repair machinery (MMR) that acts on $O^6$mG:T lesions that form upon DNA synthesis (Goldmacher et al., 1986; Kat et al., 1993)((Noonan et al., 2012; Plant and Roberts, 1971; Quiros et al., 2010).

Indeed, $O^6$mG:T lesions were found to be excellent substrates for MMR (Duckett et al., 1999; Yoshioka et al., 2006). During MMR gap-filling, the $O^6$mG:T mispair is reformed, potentially leading to another round of MMR, thus entering so-called futile MMR cycles (Kaina et al., 2007; Karran and Bignami, 1994; Olivera Harris et al., 2015; York and Modrich, 2006). The MMR cycling model has received experimental support *in vitro* (York and Modrich, 2006) and in *E. coli* (Mazon et al., 2010). Studies with synchronized cells have shown that the critical events related to cytotoxicity occur in the 2nd cell cycle post treatment (Quiros et al., 2010). However, as discussed in recent review articles, the precise mechanism by which MMR leads to DSBs has yet to be established (Gupta and Heinen, 2019; Kaina and Christmann, 2019).

While most studies have been devoted to MNU-induced cell cycle effects, in the present paper we wanted to investigate the early response to MNU treatment, i.e. in the absence of replication. We addressed this question using Xenopus egg-derived extracts, which recapitulate most forms of DNA repair (Wühr et al., 2014). Upon incubation in these extracts, plasmids treated with MNU, exhibit robust repair synthesis in the absence of replication. Repair synthesis occurs at $O^6$mG:C lesions, depends on MMR, and involves an excision tract of several hundred nucleotides. MMR events at $O^6$mG:C sites are robustly stimulated by additional processing at N-alkylation lesions, most likely via BER. Previous studies have described activation of MMR in the absence of replication in cells treated by SN1-methylating agents, a process termed noncanonical MMR (ncMMR) (Peña-Diaz et al., 2012). Interestingly, we observed replication-independent induction of DSBs in MNU-treated plasmids. The kinetics of DSB formation obeys a quadratic MNU dose-response suggesting the

involvement of two independent repair events. We propose that DSBs occur when the gap generated at a $O^6$mG adduct during MMR overlaps with a BER intermediate initiated at a N-alkyl adducts in the opposite strand.

These data reveal a novel facet of MNU-induced damage to DNA that is replication independent. Extrapolation of the *in vitro* data led us estimate that ≈ 10 DSBs per cell can be induced by a single daily dose of TMZ used in the clinic in the absence of replication.

## Results:

1. Reaction conditions leading to similar levels of DNA alkylation:

Our goal is to determine the DNA proteome for distinct alkylating agents. For sake of comparison, we needed to determine the reaction conditions for different alkylating agents that lead to similar levels of total alkylation. As a proxy for total alkylation we monitored the amount of N-alkyl adducts, namely 7mG and 3mA, that together represent > 80% of alkylation for MMS and MNU. Estimation of the N-alkyl adduct level is achieved by converting these adducts to single-stranded DNA breaks by a combination of heat depurination and alkali cleavage treatment (Maxam and Gilbert, 1977)(Figure 1-figure supplement 1A). The resulting plasmid fragmentation pattern were resolved and analyzed by agarose gel electrophoresis. The reaction conditions were adjusted (by trial and error) as to generate a median fragment size of 500 nt, corresponding to one alkylated base every 500 nucleotides on average (Figure 1-figure supplement 1A).

2. Identification of the proteins that specifically bind to DNA alkylation damage in NucleoPlasmic Extracts (NPE):

In order to identify proteins binding to $O^6$mG-containing base pairs in Xenopus egg-derived extracts, we used a recently developed plasmid pull-down procedure, IDAP, for Identification of DNA Associated Proteins (Isogawa et al., 2020; 2018). As outlined above, MNU produces 20-25-fold more $O^6$mG lesions than MMS (0.3% and 7-8% of total alkylation, respectively), while the relative amounts of N-alkyl lesions produced by the two agents is similar (> 80% of N7mG+N3mA) (Beranek, 1990). These agents react chemically with DNA under neutral pH conditions, and we established *in vitro* reaction conditions that trigger comparable levels of plasmid alkylation (see above and Fig 1-figure supplement 1A).

The pull-down procedure involves immobilization of plasmid DNA on magnetic beads by means of a triple-helix forming probe (Figure 1A) (Isogawa et al., 2020; 2018). The same amount of untreated or alkylated plasmids was coupled to magnetic beads and incubated in NucleoPlasmic Extracts (NPE) derived from Xenopus eggs (Walter et al., 1998). The reaction was stopped by dilution into a formaldehyde-containing buffer, which fixes protein-DNA complexes. After washing the beads and reversing the cross-links, the recovered proteins were visualized by silver staining following SDS-PAGE (Figure 1-figure supplement 1B). As a negative control, mock conjugated beads (noDNA control lane) exhibit low protein background illustrating efficient removal of non-specific proteins (Figure 1-figure supplement 1B). Proteins captured on the different plasmid samples were analyzed by label-free mass spectrometry as described in Material and Methods. The MS data are presented in the form of Volcano plots. When comparing MNU-treated to undamaged control plasmid, the MMR proteins (labeled in red) were highly enriched in the MNU sample (Figure 1B). All six canonical MMR proteins (MSH2, MSH3, MSH6, MLH1, PMS1 and PMS2) were specifically enriched on MNU-plasmid. These proteins form the MutSα, MutSβ, MutLα, and MutLβ heterodimers

(Jiricny, 2006). Other proteins known to participate to MMR, RAD18, POLη, EXO1 and two subunits of Pol delta (POLD2 and POLD3) were also specifically enriched on MNU-plasmid. Previously, it was shown that purified MutSα does not bind to $O^6$mG:C base pairs (Yoshioka et al., 2006). Our present experiments involve extracts containing many proteins and there is probably synergy between MutSα, MutLα (and other proteins) to achieve full MMR (Ortega et al., 2021). Activation of MMR by a single $O^6$mG:C lesion has been reported previously (Duckett et al., 1999).

It was previously noted that upon oxidative stress, produced by hydrogen peroxide treatment, RAD18 and Polη are recruited to chromatin in a MSH2-MSH6 (MutSα) dependent manner in human cells (Zlatanou et al., 2011). While MutSα, MutSβ, and MutLα functionaly participate in MMR, the role of MutLβ (MLH1-PMS1) remains unknown (Jiricny, 2006). No MMR proteins were enriched on MMS-treated plasmids (Figure 1C). As MNU treatment induces 20-30 times more $O^6$mG adducts than MMS, we postulate that recruitment of MMR proteins depends on $O^6$mG. Comparison of proteins captured on MNU- versus MMS-treated plasmids indeed reveals specific enrichment of MMR proteins. Proteins specifically recruited at N-alkyl adducts (in green in Figure 1B and 1C) are absent in the MMS versus MNU Volcano plot (Figure 1-figure supplement 1C), since N-alkyl adducts are equally present in both MMS and MNU treated plasmids.

In addition, compared to lesion-free control plasmid, some proteins were enriched on or excluded from both MMS and MNU-treated plasmids (Figure 1B and 1C, green labels). We suggest that the recruitment or exclusion of these proteins depends on the abundant 7mG and 3mA adducts formed by both MMS and MNU. The reason why BER proteins, normally involved in the repair of these N-alkyl adducts, were not captured is unclear. One possibility is that BER proteins interact too transiently with DNA to be efficiently captured.

3. Repair of alkylated plasmid DNA in NucleoPlasmic Extracts (NPE).

We next investigated the repair of DNA treated by the different alkylating agents in NPE. Plasmid was alkylated with MMS, MNU, or ENU to a density of one lesion every ≈500 nt (Figure 1-figure supplement 1A). The alkylated plasmids were incubated in NPE in the presence of $\alpha^{32}$P-dATP. These extracts contain high levels of geminin, an inhibitor of replication licensing. Therefore, any observed DNA synthesis occurs independently of DNA replication and corresponds to so-called "unscheduled DNA Synthesis" (UDS)(Figure 2A). Undamaged plasmid exhibited a low level of background DNA synthesis, whereas MNU and ENU treated plasmids sustained robust, time dependent UDS equivalent to 3-4% of the synthesis needed for a full round of replication (Figure 2B). MMS-treated plasmid exhibited UDS that was just two-fold above the background seen in undamaged plasmid (Figure 2B). Given that the assay measures incorporation of $\alpha^{32}$P-dATP, long patch BER events (Sattler et al., 2003) will be detected, while short patch BER events (1 nt patch) will only be detected at 3mA but not at 7mG adducts. The assay is clearly biased towards the detection of events such as MMR that involve repair patches hundreds of nucleotides long.

We asked whether the observed UDS in MNU- and ENU-treated plasmids was MMR dependent, as suggested by the mass spectrometry results. To test this idea, we depleted MMR proteins from extracts using antibodies (Figure 2-figure supplement 1A), whose specificity was previously validated (Kato et al., 2017; Kawasoe et al., 2016). Depletion of MLH1 or PMS2 severely reduced UDS in MNU-treated plasmid, while no reduction was observed in PMS1-depleted extracts (Figure 2-figure supplement 1B). This observation is

consistent with the fact that MutLα (composed of MLH1 and PMS2) is involved in canonical mismatch repair whereas MutLβ (composed of MLH1 and PMS1) is not (Jiricny, 2006). Aphidicolin, an inhibitor of B-family DNA polymerases (Baranovskiy et al., 2014), decreased incorporation on average 3.5-fold on MNU and ENU plasmids while it had a more modest effect on MMS-treated plasmid (1.5-fold)( Figure 2-figure supplement 1C). These results support the notion that UDS on MNU- and ENU-treated plasmids involves MMR, including a gap filling event that most likely depends on DNA Pol δ, the only B family polymerase detected in the MS analysis described above. Short-patch BER events are mediated by Pol β (X family) that are insensitive to aphidicolin. The modest sensitivity of MMS-induced UDS to aphidicolin is probably due to a fraction of BER events that belong to the long-patch BER pathway mediated Pol δ/ε (Sattler et al., 2003).

We wanted to estimate the average amounts of DNA synthesis associated with MMR at $O^6$mG:C sites and BER at N-alkyl sites, respectively. At the 90 min time point (i.e. at near plateau value), the difference in UDS between MNU- and MMS-treated plasmids, i.e. attributable to repair at $O^6$mG:C sites, was equivalent to ≈ 3.1% of the input DNA (Figure 2B) or ≈270 nt (pBR322 plasmid is 4363 bp long). With an estimated ≈ 1.7 $O^6$mG adducts per plasmid, the average repair patch per $O^6$mG adduct is ≈ 160 nt provided all $O^6$mG lesions are targeted by MMR. Evidence obtained with G:T and $O^6$mG:T constructs (see below) indicates that, under present experimental conditions, only about ≈30% of $O^6$mG are substrates for MMR, suggesting that on average a MMR patch is ≈ 500 nt long. Importantly, the MGMT inhibitor Patrin-2 had no effect on UDS of MNU-treated plasmid, even at a dose of 200 μM (data not shown). Surprisingly, inhibition of MGMT by Patrin-2 was previously shown to occur in Xenopus extracts (Olivera Harris et al., 2015). Two possibilities may account for the lack of any measurable effect of MGMT inhibition: i) the number of MGMT molecules present in the extract is small compared to the number of $O^6$mG lesions introduced in the incubation mix or ii) our batch of Patrin inhibitor is inactive. In all cases, if partial demethylation of $O^6$mG by MGMT occurs, the observed amount of UDS would be <u>under-estimated</u>. Thus, the conclusion reached in the paper, namely that $O^6$mG:C sites are substrates for MMR, remains correct.

With respect to N-alkyl adduct repair in MMS-plasmid, repair synthesis above the lesion-free DNA control is equivalent to ≈0.5% of input DNA (Figure 2B), corresponding to 43 nt total synthesis per plasmid. With ≈ 17 N-alkyl adducts per plasmid, the average DNA synthesis patch per adduct, in case all N-alkyl lesions are repaired, is ≈2.6 nt, a value consistent with a mixture of long (≈ 2-8 nt) and short patch (1nt) BER events at N-alkyl adducts. In summary, the average DNA repair patch sizes at $O^6$mG:C (≈500 nt) and N-alkyl (2-3 nt) sites are compatible with MMR and BER, respectively.

To learn more about UDS in this system, we analyzed repair products via gel electrophoresis. Plasmid pBR322 treated with MMS or MNU was incubated in NPE, supplemented or not with Aphidicolin in the presence of $\alpha^{32}$P-dATP, and analyzed on a neutral agarose gel. As already noticed above (Figure 2-figure supplement 1C), addition of Aphidicolin (Aph) led to more severe reduction in incorporation into MNU- (≈3.7-fold) compared to MMS-treated plasmid (≈1.6-fold) (Figure 2C). We also note that in MNU-treated plasmids, in the absence of Aph, open circular repair products were three-fold more abundant than closed circular products (Figure 2C, $^{32}$P image). This observation suggests that MMR repair was complete in only ≈25% of plasmid molecules while 75% of molecules contained at least one nick (or a gap). Interestingly, there was a ≈50% loss of total DNA in the MNU + Aph lane compared to the other lanes, suggesting massive DNA degradation in NPE

due to polymerase inhibition by Aph. Indeed, the observed DNA degradation can specifically be linked to repair events as the loss in radioactivity in MNU lanes -Aph versus + Aph is >70% (Figure 2C, $^{32}$P image). Under alkaline loading conditions (Figure 2D), repair products ($^{32}$P image) in MNU-treated plasmids appeared mostly as a single-stranded linear band form. In addition, there was a large smear (>25% of material) of shorter fragments. These results show that most plasmids contain 1 nick and some contain several nicks. In the +Aph samples, the open circular (oc) form, seen in the gel loaded under neutral conditions (Figure 2C), disappear under alkali loading conditions (Figure 2D). This suggests that these oc molecules (Figure 2C) contain many nicks that run as short fragments upon denaturation. In conclusion, MNU-treated plasmids undergo robust repair synthesis that is more sensitive to aphidicolin inhibition than MMS-treated plasmids.

We next examined O$^6$mG-induced DNA synthesis in a different extract, namely High-Speed Supernatant (HSS) of total egg lysate. Unmodified pBR322 (DNA0) or treated with MNU to an extent of ≈1 N-alkyl adduct/500nt, were incubated in the presence of $\alpha^{32}$P-dATP. Repair synthesis was monitored at room temperature as a function of time using the spot assay described above (Figure 2A). In HSS extract, MNU-treated plasmid does not exhibit significant repair synthesis (Figure 2-figure supplement 2), in contrast to the robust repair synthesis seen in NPE extract (Figure 2B). Although, HSS contains lower concentrations of most DNA repair enzymes compared to NPE, HSS was shown to be proficient for MMR at a single O$^6$mG provided a nick is present in proximity (Olivera Harris et al., 2015). We reasoned that HSS might not contain adequate concentrations of the DNA glycosylase AAG, which initiates BER at N-alkyl sites. When HSS extract was supplemented with purified AAG glycosylase (150nM) (NEB, Biolabs), robust repair synthesis is observed in MNU-treated plasmid (Figure 2-figure supplement 2). These observations suggest the involvement of BER in stimulating MMR at O$^6$mG lesions.

4. MMR at single O$^6$mG-containing base pairs is enhanced by the presence of N-alkylation adducts.

Next, we explored a possible crosstalk between repair pathways acting on alkylated DNA. In MNU-treated plasmid, there is on average one O$^6$mG adduct for every 9-10 N-alkyl adducts (Beranek, 1990). To investigate the repair response triggered by a single O$^6$mG:C lesion alone or in the presence of additional N-alkyl adducts, we implemented a reconstitution experiment. For that purpose, a single O$^6$mG:C construct (mGC) (Isogawa et al., 2020) was treated with MMS to introduce ≈ 9-10 N-alkyl adducts per plasmid molecule, generating plasmid mGC+MMS, that is expected to recapitulate adduct distribution found in MNU-treated plasmids. Control plasmid GC was treated with the same concentration of MMS, to generate GC+MMS. These *in vitro* manipulations did not affect plasmid topology as all four constructs exhibit a similar migration pattern (Figure 3-figure supplement 1A).

Plasmid constructs GC and mGC and the corresponding two MMS-treated constructs (GC+MMS and mGC+MMS) (Figure 3A), were incubated with NPE in the presence of $\alpha^{32}$P-dATP to monitor repair synthesis (i.e. UDS). We observed, incorporation of radioactivity specifically attributable to the single O$^6$mG:C lesion (compare mGC to GC in Figure 3B). Activation of MMR by a single O$^6$mG:C lesion has been reported previously (Duckett et al., 1999). The specific involvement of MMR for O$^6$mG dependent incorporation was re-assessed, by incubating the single adducted O$^6$mG:C construct in MLH1-depleted NPE extract; radioactive incorporation above background was fully abolished in mGC plasmid (Figure 3-

figure supplement 1E). How MMR may get engaged in a repair reaction on a closed circular template will be considered in the Discussion section.

Importantly, repair synthesis, due to the single $O^6$mG:C lesion, is strongly enhanced by the presence of MMS adducts (compare mGC+MMS to GC+MMS in Figure 3B). At the 2h time point, incorporation, above background, due to the single $O^6$mG, expressed in % replication equivalent, represents 0.64% (difference between mGC and GC), while it amounts to 1.85% in the presence of MMS lesions (compare mGC+MMS with GC+MMS). One can thus estimate that, incorporation due to a single $O^6$mG lesion, is stimulated about 2.9-fold (1.85/0.64) by the presence in *cis* of MMS adducts (Figure 3B).

Finally, we wanted to compare the relative MMR repair efficiencies triggered by $O^6$mG:C and $O^6$mG:T (or GT) mismatches (Figure 3A and B). These constructs were used as single adducted constructs or after additional reaction with MMS similarly to the procedure described for the corresponding GC or mGC constructs. The main observation is that GT containing constructs trigger a much stronger MMR response than their GC counterparts (Figure 3B). In the absence of MMS, at the 120' time point, the level of UDS in mGC represents 23% of the level in mGT. In the presence of MMS, at the 120' time point, the level of UDS in mGC+MMS represents 38% of the level in mGT+MMS. In conclusion, supposing that 100% of mGT mispairs are fully repaired, the extent of mGC repair would be in the range of 30%.

5. Nucleotide incorporation occurs in the vicinity of the single $O^6$mG adduct.

The plasmids described above were incubated in $\alpha^{32}$P-dATP supplemented NPE for 2h, purified plasmids and analyzed by agarose gel electrophoresis (Figure 3C). Covalently closed circular (ccc) and relaxed forms (oc) were quantified in each lane (Figure 3C). In the presence of MMS adducts, the single $O^6$mG:C lesion contributes to a 2.8-fold increase in radioactive incorporation compared to its contribution in the absence of MMS (Figure 3C) in good agreement with the UDS data (Figure 3B).

We wanted to map the repair patches with respect to the $O^6$mG adduct position by restriction enzyme analysis. Digestion of the purified plasmids with *BmtI* and *BaeGI* restriction enzymes, generates fragment S (589 bp) that encompasses the $O^6$mG:C site and fragment L (1525 bp) (Figure 3-figure supplement 1B). Following separation by agarose gel electrophoresis, the DNA was imaged by ethidium bromide fluorescence and $^{32}$P autoradiography (Figure 3-figure supplement 1C). For each fragment, we determined its specific activity by dividing the radioactivity signal by its amount as determined from the ethidium bromide image (Figure 3-figure supplement 1D). As expected, the specific activities of S and L fragments were similar in GC (random background incorporation: 0.125±0.015 AU (arbitrary units)) and MMS treated (GC+MMS) (0.235±0.025 AU) control plasmids. In GC+MMS, the specific activity was slightly higher than in control plasmid, probably reflecting BER-mediated incorporation at randomly distributed N-alkyl adducts. In the two $O^6$mG:C containing plasmids (mGC and mGC+MMS), the S fragment exhibits a significantly higher specific activity than the L fragment indicating that MMR activity is centered around the $O^6$mG:C site. In the absence of MMS, incorporation in mGC above background (dotted line in Figure 3-figure supplement 1D), attributable to $O^6$mG, amounts to 0.065 and 0.495 AU (arbitrary units) for L and S fragments, respectively. Similarly, in the presence of random MMS lesions (mGC+MMS), incorporation, above background (dotted line in Figure 3-figure supplement 1D), attributable to $O^6$mG amounts to 0.115 and 1,17 AU for L and S fragments, respectively. These results clearly show that $O^6$mGC induced repair essentially takes place

within the S fragment, with only modest spill-over into the L fragment (10-15%). This observation appears to be good agreement with the estimated average MMR patch size (~500 nt). Thus, MMS adducts do not modify the repair pattern, i.e. the relative distribution of $^{32}$P incorporation in S and L fragments, but they increase the frequency of repair centered at O$^6$mG sites. In conclusion, we show that stimulation of repair synthesis by N-alkyl adducts specifically occurs in the vicinity of the O$^6$mG adducts, illustrating that processing of N-alkyl adducts enhances MMR activity.

6. MNU-treated plasmids undergo double-strand breaks during incubation in extracts.

Work in *E. coli*, provided elegant genetic evidence that the cytotoxicity of alkylating agents forming O$^6$mG adducts (such as N-methyl-N'-nitrosoguanidine and MNU), including formation of replication-independent DSB, was strongly influenced by the status of the MMR pathway (Karran and Marinus, 1982; Nowosielska and Marinus, 2008). We wondered whether MNU can induce formation of DSBs independently of DNA replication. To increase the sensitivity of our assay towards DSB detection, we used a larger plasmid, pEL97 (11,3 kb), and treated it with MMS or MNU to introduce one alkylation event on average every 500 nt (Figure 4-figure supplement 1). We also treated one sample with double the concentration of MNU to achieve a 2-fold higher lesion density. Quantification of N-alkyl adducts by alkaline cleavage and subsequent agarose gel electrophoresis led to the expected lesion density of one N-alky adduct every 500 nt for MMS and MNU+, and one N-alky adduct every 250 nt MNU++ (Figure 4-figure supplement 1C).

Alkylated and control plasmids (Figure 4-figure supplement 2A) were incubated in NPE for 60' in the presence of $\alpha^{32}$P-dATP, resolved by agarose gel electrophoresis, and visualized by ethidium bromide staining and $^{32}$P imaging (Figure 4A). Both MMS and MNU caused substantial conversion of the plasmid from supercoiled to open circular form, as expected during repair synthesis. Consistent with our results above, MNU induced much more repair synthesis than MMS. Strikingly, in both ethidium bromide and $^{32}$P images, linear plasmid was detected after exposure to MNU, but not MMS. For a two-fold increase in MNU exposure, the linear plasmid band increased ≈4-fold (Figure 4B). This quadratic dose-response strongly suggests that DSBs occur as a consequence of two independent repair events at neighboring lesions, for example a BER event at an N-alkyl adduct leading to a nick in one strand that is encountered by a gap formed by an MMR event initiated at a O$^6$mG site in the opposite strand (Figure 5). To reveal single-strand breaks, the same samples were denatured prior to native gel electrophoresis (Figure 4-figure supplement 2B). In the MNU++ sample, no linear single-stranded DNA (ssDNA) is left, all the DNA molecules running as a smear centered around the 3000 nt position (Figure 4-figure supplement 2B). The observed smear reveals that the double-stranded DNA running as open circular plasmid molecules in the neutral loading gel (Figure 4A), contain each on average 3-4 nicks per plasmid strand. The data reveal that repair of MNU-treated plasmid in NPE causes SSBs, and that once the density of SSBs is high enough, DSBs result.

## Discussion:

With respect to the biological responses to SN1 alkylating agents most attention has so far been devoted to responses that occur in the first or second cell cycle following treatment as mentioned in the introduction (Noonan et al., 2012; Plant and Roberts, 1971; Quiros et al., 2010).

In the present paper, we focus on early processing of DNA alkylation adducts by repair pathways before the event of replication. Interestingly, we identify the formation of DSB as the result of a putative crosstalk between repair pathways.

*Late responses to SN1 agents:*

Response of cells to SN1 methylating agents was shown to be initiated at $O^6$mG:T mispairs that form upon DNA replication of $O^6$mG containing DNA template and shown to involve the MMR machinery (Goldmacher et al., 1986) (Day et al., 1980; Karran et al., 1993; Yarosh et al., 1983). The $O^6$mG:T mispair is efficiently recognized by MutSα, the key MMR initiator protein. Following removal of the nascent T residue across $O^6$mG, T will be re-inserted at high frequency during the MMR gap-filling step thus re-forming the initial $O^6$mG:T mispair. This iterative process, called "futile cycling", has received experimental support (Mazon et al., 2010; York and Modrich, 2006). However, it is not yet clear how these futile cycles lead to DSBs (Ochs and Kaina, 2000), apoptosis and cell death (Gupta and Heinen, 2019; Kaina and Christmann, 2019). Two mutually non-exclusive models have been proposed, i) a direct model where the encounter of the replication fork with the MMR intermediates leads to fork collapse and to subsequent cytotoxic events; ii) a signaling model where the MutSα complex acts as a sensor leading to ATR recruitment and subsequent initiation of the ATR-Chk1 signaling pathway (Duckett et al., 1999; Yoshioka et al., 2006). However, presently there is more evidence that the critical cytotoxic response to methylating agents is the consequence of direct MMR processing rather than being mediated by a mere signaling model (Cejka and Jiricny, 2008; Karran, 2001; Liu et al., 2010; York and Modrich, 2006).

*Early responses to SN1 agents:*

While all biological responses described above require replication of $O^6$mG containing DNA templates as the first step, we wanted to investigate the processing of MNU-alkylated DNA in the absence of replication. Interestingly, we detect robust, MMR-dependent, UDS upon incubation of MNU-treated plasmid in NPE. This observation reveals that, not only are $O^6$mG:C lesions recognized by MutSα as previously noted (Duckett et al., 1999; Karran et al., 1993), but that the whole MMR repair process is engaged and proceeds to completion. We would also like to stress the high sensitivity of the pull-down assay with respect to MMR proteins capture. Indeed, the whole MMR machinery is enriched (Figure 1B) using a plasmid that on average carries only 2-3 $O^6$mG lesions/plasmid. In striking contrast, despite their abundance, ≈26 N-alkyl lesions/plasmid, N-alkyl lesions only recruit few specific proteins (Figure 1C).

We wanted to investigate the potential effect that N-alkyl adducts may have on MMR processing at $O^6$mG:C base pairs. For that purpose, we compared a plasmid with a single site-specific $O^6$mG:C lesion to a plasmid additionally treated with MMS, an agent known to induce essentially only N-alkyl adducts. The MMS treatment was adjusted as to produce the same amount of N-alkyl adduct as generated by MNU. The single-adducted $O^6$mG:C plasmid triggered MMR mediated repair synthesis centered around the $O^6$mG adduct. Interestingly, the presence of randomly distributed N-alkyl adducts led to a 3-fold increase of the MMR repair activity in the vicinity of the $O^6$mG adduct. These data raise two questions, first, how does the MMR machinery get engaged in ccc plasmid and how is MMR activity further stimulated by N-alkyl adducts? In current models, functional engagement of MMR involves a mismatch recognized by MutSα, subsequent recruitment of MutLα and PCNA (Jiricny, 2006). Loading of PCNA by RFC normally requires a single-stranded nick but it was also shown to

occur, although less efficiently, on ccc DNA (Pluciennik et al., 2013; 2010). Under these conditions, PCNA loading and MMR processing lack strand directionality. With respect to the mechanism by which MMR activity, at a single $O^6$mG:C lesion, becomes stimulated several folds by the presence of N-alkyl adducts, we propose that processing of N-alkyl adducts by BER creates repair intermediates (nicks) that stimulate PCNA loading. It was previously shown that BER intermediates formed at oxidized purines or U residues can stimulate MMR processing (Repmann et al., 2015; Schanz et al., 2009).

*DSB form in MNU-treated DNA in the absence of replication: potential therapeutic significance*.

Interestingly, incubation of MNU-treated plasmid in extracts leads to DSBs (Figure 4) that arise with a quadratic dose response suggesting the occurrence of two independent repair activities taking place simultaneously in opposite strands at lesions that may be up to several hundred nucleotides apart (see scenario in Figure 5). Similarly, *in vitro* processing of neighboring G/U mispairs by BER and by non-canonical MMR was shown to lead to DSBs (Bregenhorn et al., 2016).

The extent of DNA alkylation triggered by MNU *in vitro*, as deduced from our alkaline cleavage determination, fits surprisingly well with the amount of alkylation induced by TMZ in cell at equal concentrations (Moody and Wheelhouse, 2014) (Kaina, personal communication). According to the model (Figure 5), formation of a DSB may occur when an N-alkyl lesion is located within the repair track mediated by MMR at a $O^6$mG:C site. In the clinic, a daily dose of TMZ results in 50μM serum concentration and was shown to induce $5.2x10^4$ and $7.3x10^5$ O-alkyl and N-alkyl lesions per human genome, respectively (Kaina, personal communication). We can estimate the number of events (per genome) where an N-alky lesion is located within 500 nt on either side of a $O^6$mG:C site. Given the N-alkyl lesion density ($7.3x10^5/6x10^9 = 1.2x10^{-4}$), the probability of presence of an N-alky lesion within an MMR track is 0.12. In other words, among the $5.2x10^4$ $O^6$mG lesions, ≈6,240 are likely to contains a N-alkyl lesion within a 1000 nt excision track. We will refer to such a lesion configuration as a "Lesion Arrangement at-risk" for DSB formation.

Let us now estimate the level of DSB that may occur in a human genome, by extrapolation of our *in vitro* data. In the present work, ≈6% of plasmid DNA (11.3 kb) treated by MNU at 2mM exhibit a DSB (Figure 4). The observed amount of DSBs may in fact only reflect a steady state level since efficient re-ligation mechanisms are known to operate in NPE (Graham et al., 2016). As MNU and TMZ exhibit similar reactivities (Moody and Wheelhouse, 2014)(Kaina personal communication) a dose of 2mM MNU would lead to $3x10^9$ x 0.06 / 11300= 16,000 DSBs per genome. In the clinic, the level of TMZ in the serum reaches up to 50μM, i.e. 40 times less than the 2mM dose used *in vitro*. Given the quadratic dose-response, the estimated amount of DSBs per genome would be 1600 times less, i.e. ≈10. Lets note that the conversion rate of a Lesion Arrangement at-risk into an actual DSB appears to be quite low (10/6,240 ≈0,16%), reflecting the requirement for simultaneous occurrence of two repair events (MMR and BER).

The alkylating agent Temozolomide (TMZ), a chemical mimic of MNU, is presently the first-line and only anti-cancer drug in glioblastoma therapy (Moody and Wheelhouse, 2014). The cytotoxic mode of action of alkylating agents such as TMZ is believed to result from iterative MMR cycles. Iterative MMR cycles are deemed to lead to double-strand breaks (DSB) via a mechanism that is not yet established (Ochs and Kaina, 2000). Indeed, it is not known whether DSB's occur spontaneously at these sites or as a consequence of the replication fork

running into the MMR intermediates. Induction of these putative DSB's is presently thought to be the primary mode-of-action of TMZ when administered to patients with glioblastoma. Understanding both early and late cellular responses to MNU/TMZ appears thus to be critical. During cancer treatment, a dose of TMZ is delivered concomitantly with a radiotherapy session daily, for 6 weeks (for a recent review see Strobel et al., 2019). As estimated above, a daily dose of TMZ, may lead to a ≈10 DSBs/cell resulting from BER/MMR crosstalk, a number comparable to the number of DSBs induced by 0.5-1 Gy of IR. Moreover, it was established empirically, that the treatment TMZ plus radiotherapy exhibits supra-additive cytotoxicity as long as TMZ administration *precedes* radiotherapy (Bobola et al., 2010). Our data may provide some rational for this empirically determined regimen. Indeed, the single-stranded DNA stretches formed at early time points during MMR processing at $O^6$mG:C sites (step 3 in Figure 5) constitute preferential targets for the conversion of the numerous single-stranded breaks induced by ionizing radiations (IR) into DSBs, thus providing an explanation for the observed supra-additivity in the treatment when TMZ *precedes* IR. A commonly used radiotherapy session involves an IR dose of 2 Gy that predominantly induces ≈2000 single-strand breaks and ≈40 DSBs/cell.

As the majority of cells in a glioblastoma tumor are not proliferating, insight into attacking non-dividing cells might be very useful in treating this almost always fatal tumor. This pre-replicative mechanism for TMZ cytotoxicity will need to be investigated in cellular systems. In conclusion, the present work offers a novel mechanistic insight into the cytotoxicity of TMZ via induction of DSBs, at early time points following exposure, before replication. This early response comes in complement to the late, replication and cell cycle dependent, responses that have been described over the years.

Acknowledgements: We thank Johannes Walter (Harvard Medical School) for providing space, advice and materials. Paul Modrich (Duke Univ) and Bernd Kaina (Medical Univ, Mainz) for insightful reading and suggestions.

Funding:
This work was partially supported by NIH/NIGMS grant R01 GM132129 (to JAP) and MEXT/JSPS KAKENHI JP20H03186 and JP20H05392 (to TT).

## Material and Methods.

Plasmids: alkylated plasmids as used in the present paper are outlined below:

| name | Size (kb) | Assay |
|---|---|---|
| pAS200.2 | 2,1 | Site-specific $O^6$mG lesion |
| pBR322 | 4,3 | Random alkylation / UDS repair assay |
| pAS04 | 6,5 | IDAP pull-down assay / MS analysis of bound proteins |
| pEL97 | 11,3 | Random alkylation / UDS assay / post incubation analysis |

Akylation reactions are conducted as indicated in Fig 1-figure supplement 1, at a plasmid concentration of 10ng/μl in CE buffer (citrate 10mM pH7, EDTA 1mM) + 10% DMSO final.

Alkylation reactions are terminated by addition of STOP buffer (5x: 1.5M sodium acetate, 1M mercapto-ethanol) followed by ethanol precipitation. The DNA pellet is washed with ethanol 90% and re-dissolved in TE at 50ng/µl.

Cleavage reactions at 7-alkylG and 3-alkylA adducts. Alkylated plasmids (50ng in 10µl of CE buffer) are first incubated for 90°C during 15' at pH7 (PCR machine). Following addition of 1µl of NaOH 1N, the sample is further incubated at 90°C for 30'. Following addition of 2µl of alkaline 6x loading buffer (NaOH 300mM, EDTA 6mM, Ficoll (Pharmacia type 400) 180mg/ml, 0.15% (w/v) bromocresol green, 0.25% (w/v) xylene cyanol), the cleaved plasmid samples are loaded on a neutral agarose gel. (Figure 1-figure supplement 1A)

NPE and HSS Xenopus extracts: Two type of extracts derived from *Xenopus laevis* eggs are used throughout the paper, namely NucleoPlasmic Extracts (NPE) and High-Speed Supernatant (HSS) as described previously (Lebofsky et al., 2009).

Western Blot: Antibodies against Mlh1, Pms2 and Pms1 as previously described (Kato et al., 2017; Kawasoe et al., 2016). For western blotting primary antibodies used at 1:5000 dilution.

Single adducted plasmids. Covalently closed circular plasmids containing a site-specific $O^6$mG:C base pair (plasmid mGC) and the corresponding lesion-free control (plasmid GC) were constructed. We also constructed similar plasmids with a single GT or a single $O^6$mG:T mismatch located at the same position (plasmids GT and mGT, respectively). All constructs were derived from plasmid vector pAS200.2 (2.1 kb) (Isogawa et al., 2020).

Plasmid immobilization on magnetic beads and pull-down procedure.
Alkylated plasmids samples (250 ng of each -MMS, -MNU and -ENU), as well as a non-alkylated control sample (DNA0) were immobilized on magnetic beads at a density of 10 ng plasmid / µl of M280 bead slurry using a triple helix-based capture methodology (Isogawa et al., 2018). The TFO1 probe used here is 5' Psoralen – C6 – TTTTCTTTTCTCCTCTTCTC– C124 – Desthiobiotin (20 mer) with C124: hexaethylene glycol ×6. Underlined C is for 5mC; it was synthesized by using DNA/RNA automated synthesizer and purified with conventional methods (Nagatsugi et al., 2003).

Immobilized plasmid DNA are incubated in NPE extract (final volume 16µl) for 10 min at room temperature under mild agitation. To monitor non-specific protein binding to beads, we included a negative control (noDNA sample) containing the same amount of M280 beads treated under the same conditions but in absence of plasmid DNA. Reactions were stopped by addition of 320µl of a 0.8% HCHO solution to cross-link the proteins-DNA complexes for 10 min at room temperature. The beads were subsequently washed at RT with 200µl of 100mM NaCl containing buffer (ELB buffer), re-suspended in 70µl of Extract Dilution buffer and layered on top of a 0.5M sucrose cushion in Beckman Coulter tubes (Ref: 342867). The beads were quickly spun trough the cushion (30 sec at 10 000 rpm), the bead pellet is re-suspended into 40µl of ELB sucrose and further analyzed by PAGE or by MS.

PAGE / silver staining:
An aliquot of each incubation experiments, corresponding to 30 ng of immobilized plasmid was treated at 99°C for 25 min in a PCR machine to revert HCHO cross-linking in LLB, 50 mM

DTT. Samples were loaded on a 4-15% PAGE (Biorad pre-cast) gel at 200 volts for 32min and stained using the silver staining kit (silver StainPlus, Biorad).

Incorporation of $\alpha^{32}$P-dATP into DNA: spot assay.
Plasmids are incubated in nuclear extracts supplemented with $\alpha^{32}$P-dATP; at various time points, an aliquot of the reaction mixture is spotted on DEAE paper (DE81). The paper is soaked in 100ml 0.5M Na2HPO4 (pH≈9), shacked gently for 5' before the buffer is discarded; this procedure is repeated twice. Finally, the paper is washed an additional 2 times in 50ml ethanol, air dried and analyzed by $^{32}$P imaging and quantification. The extent of DNA repair synthesis is expressed as a fraction of input plasmid replication (i.e. 10% means that the observed extent of repair synthesis is equivalent to 10% of input plasmid replication). This value is determined knowing the average concentration of dATP in the extracts (≈50μM) and the amount of added $\alpha^{32}$P-dATP.

Mass Spectrometry. Label-free mass spectrometry analysis was performed using on-bead digestion. In solution digestion was performed on beads from plasmid pull-downs. We added 20 µl of 8 M urea, 100 mM EPPS pH 8.5 to the beads, then 5mM TCEP and incubated the mixture for 15 min at room temperature. We then added 10 mM of iodoacetamide for 15min at room temperature in the dark. We added 15 mM DTT to consume any unreacted iodoacetamide. We added 180µl of 100 mM EPPS pH 8.5. to reduce the urea concentration to <1 M, 1 µg of trypsin, and incubated at 37°C for 6 hrs. The solution was acidified with 2% formic acid and the digested peptides were desalted via StageTip, dried via vacuum centrifugation, and reconstituted in 5% acetonitrile, 5% formic acid for LC-MS/MS processing.

All label-free mass spectrometry data were collected using a Q Exactive mass spectrometer (Thermo Fisher Scientific, San Jose, CA) coupled with a Famos Autosampler (LC Packings) and an Accela600 liquid chromatography (LC) pump (Thermo Fisher Scientific). Peptides were separated on a 100 µm inner diameter microcapillary column packed with ~20 cm of Accucore C18 resin (2.6 µm, 150 Å, Thermo Fisher Scientific). For each analysis, we loaded ~2 µg onto the column. Peptides were separated using a 1 hr gradient of 5 to 29% acetonitrile in 0.125% formic acid with a flow rate of ~300 nL/min. The scan sequence began with an Orbitrap $MS^1$ spectrum with the following parameters: resolution 70,000, scan range 300−1500 Th, automatic gain control (AGC) target $1 \times 10^5$, maximum injection time 250 ms, and centroid spectrum data type. We selected the top twenty precursors for $MS^2$ analysis which consisted of HCD high-energy collision dissociation with the following parameters: resolution 17,500, AGC $1 \times 10^5$, maximum injection time 60 ms, isolation window 2 Th, normalized collision energy (NCE) 25, and centroid spectrum data type. The underfill ratio was set at 9%, which corresponds to a $1.5 \times 10^5$ intensity threshold. In addition, unassigned and singly charged species were excluded from $MS^2$ analysis and dynamic exclusion was set to automatic.

Mass spectrometric data analysis**.** Mass spectra were processed using a Sequest-based in-house software pipeline. MS spectra were converted to mzXML using a modified version of ReAdW.exe. Database searching included all entries from the *Xenopus laevis*, which was concatenated with a reverse database composed of all protein sequences in reversed order. Searches were performed using a 50 ppm precursor ion tolerance. Product ion tolerance was set to 0.03 Th. Carbamidomethylation of cysteine residues (+57.0215Da) were set as static modifications, while oxidation of methionine residues (+15.9949 Da) was set as a variable modification. Peptide spectral matches (PSMs) were altered to a 1% FDR (Elias and Gygi,

2010; 2007). PSM filtering was performed using a linear discriminant analysis, as described previously (Huttlin et al., 2017), while considering the following parameters: XCorr, ΔCn, missed cleavages, peptide length, charge state, and precursor mass accuracy. Peptide-spectral matches were identified, quantified, and collapsed to a 1% FDR and then further collapsed to a final protein-level FDR of 1%. Furthermore, protein assembly was guided by principles of parsimony to produce the smallest set of proteins necessary to account for all observed peptides.

Legend to Figures:

Figure 1. Pull-down of proteins that bind to alkylated- versus untreated-plasmid DNA.

A. Experimental workflow. plasmid DNA (pAS04, 6.5kb) was treated with alkylating agents under conditions leading to a similar extent of N-alkylation (≈ one alkaline cleavage site every 500 nt, (Figure 1-figure supplement 1A). Immobilized plasmid DNA were incubated in Xenopus NucleoPlasmic Extracts (NPE) for 10 min at room temperature under mild agitation. The reaction was stopped by addition of formaldehyde (0.8% final) to cross-link the proteins-DNA complexes. The beads were processed and analyzed by PAGE or by MS as described in Material and Methods.

B. Relative abundance of proteins captured on MNU-treated versus untreated DNA0. Proteins captured on equal amounts of MNU- or untreated plasmid were analyzed by label-free MS in triplicates. For all proteins, average spectral count values in the MNU-treated plasmid sample were divided by the average spectral count values in the DNA0 sample. The resulting ratio is plotted as its $\log_2$ value along x-axis. The statistical significance of the data is estimated by the p value in the Student test and plotted as the $-\log_{10}p$ along y-axis. Proteins enriched on MNU versus untreated plasmid DNA appear in the right-side top corner and essentially turn out to be MMR proteins labelled in red (Figure 1B). Data shown are analyzed using Xenbase data base.

C. Relative abundance of proteins captured on MMS-treated versus untreated DNA0. Proteins captured on equal amounts of MMS- or untreated plasmid were analyzed by label-free MS in triplicates. The data are analyzed and plotted as in panel B for MNU using Xenbase data base. Proteins (labeled in green in Figure 1B and 1C) are found enriched or excluded in both MMS versus DNA0 and MNU versus DNA0 plasmids. We suggest these proteins are recruited or excluded from binding to DNA by the abundant class of N-alkylation adducts that both MMS- and MNU-treated plasmids share in common (~27 N-alkyl adducts per plasmid).

Figure 1-figure supplement 1.

A. Alkylation reaction conditions and alkaline cleavage. The alkylation reaction conditions (concentration, reaction temperature and time), were adjusted by successive trials until an average of one N-alkyl adduct per 500 nt was reached. The desired level of alkylation (≈1 N-alkyl adduct / 500nt) was attested using the alkaline cleavage procedure, followed by neutral agarose gel electrophoresis (for details, see Material and Methods).

B. PAGE analysis and silver staining of the captured proteins. Proteins captured on equal amount of immobilized plasmid DNA incubated in NPE (as described in Figure 1A) were resolved by denaturing gel electrophoresis and silver stained. Samples, corresponding to ≈ 30 ng of immobilized input plasmid DNA, were loaded on a 4-15% PAGE (Biorad pre-cast) gel, run at 200 volts for 32min and silver stained. Lanes DNA0, MMS, MNU and ENU display a complex pattern of proteins (total amount of proteins per lane estimated at 100-200 ng). To monitor non-specific protein binding to beads, we include a negative control containing the same amount of M280 beads in the absence of plasmid DNA (noDNA). Importantly, in the noDNA lane only a low amount of residual protein is visible indicating efficient removal of non-specifically protein binding during the washing procedure.

C. Relative abundance of proteins captured on MNU- versus MMS-treated plasmid. Proteins captured on equal amounts of MNU- or MMS-treated plasmid were analyzed by label-free MS

in triplicates. The data are analyzed and plotted as described in Figure 1B using Xenbase data base. Proteins enriched on MNU versus MMS-treated DNA appear in the right-side top corner and essentially turn out to be MMR proteins labelled in red (Figure 1B).

Figure 2. DNA repair synthesis in alkylated and undamaged control plasmid DNA in NPE extracts.

A. Outline of the spot assay. Plasmids were incubated in nuclear extracts supplemented with $\alpha^{32}$P-dATP; at various time points, an aliquot of the reaction mixture was spotted on DEAE paper (see Material and Methods). The dot blot that is shown for sake of illustration only.

B. Plasmid DNA pBR322 (4.3kb) samples, modified to a similar extent with -MMS, -MNU and -ENU, were incubated in NPE supplemented with $\alpha^{32}$P-dATP at room temperature; incorporation of radioactivity was monitored as a function of time using the spot assay described above (Figure 2A). Undamaged plasmid DNA0 was used as a control. At each time point, the average values and standard deviation from three independent experiments were plotted. The y-axis represents DNA repair synthesis expressed as a fraction of input plasmid replication (i.e. 10% means that the observed extent of repair synthesis is equivalent to 10% of input plasmid replication). This value was determined knowing the average concentration of dATP in the extract (50μM) and the amount of added $\alpha^{32}$P-dATP.

C. MMS and MNU-treated plasmids were incubated in NPE, supplemented or not, by aphidicolin (150μM final). After 1 h incubation, plasmids were purified and analyzed by agarose gel electrophoresis under neutral loading conditions. The gel was imaged by fluorescence (left: ethidium bromide image) and by autoradiography (right $^{32}$P image). The number below each lane indicates the total amount of signal per lane (expressed in AU). Aphidicolin treatment decreases incorporation into MNU-treated plasmid close to 4-fold, while it affected incorporation into MMS-treated plasmid only 1.6-fold.

D. Samples as in C. Gel loading is performed under alkaline conditions to denature DNA before entering the neutral agarose gel allowing single-stranded nicks present in DNA to be revealed. The number below each lane indicates the amount of signal per lane (AU).

Figure 2-figure supplement 1. Involvement of Mismatch repair in repair synthesis and effect of aphidicolin.

A. Analysis by WB of the NPE extracts depleted for MMR proteins. Antibodies against Mlh1, Pms2 and Pms1 as previously described (Kato et al., 2017; Kawasoe et al., 2016). Extracts were depleted, with the respective antibodies, for three rounds at 4C° at a ratio beads: antibody: extract = 1 :3 :5.

B: Depletion experiments show that $\alpha^{32}$P-dATP incorporation into MNU-plasmid is mediated by Mismatch Repair. NPE was depleted by antibodies against Pms1, Pms2, Mlh1 or mock depleted. Upon incubation at room temperature in the different NPE extracts, incorporation of $\alpha^{32}$P-dATP in MNU- plasmid was monitored by the spot assay as a function of time. At each time point, the average values and standard deviations from two independent experiments were plotted. As expected from previous data (Figure 2B), robust incorporation was observed for MNU-plasmid incubated in mock-depleted extract. In contrast, radioactive dATP incorporation was severely reduced when the plasmid was incubated in extracts depleted with antibodies against Mlh1 or Pms2. These data strongly suggest that the incorporation seen in mock depleted NPE is mediated by MMR, as both Mlh1 and Pms2 assemble into the

functional MMR complex MutLα. In contrast, depletion with antibodies against Pms1 did not affect incorporation kinetics as Pms1 is reported not to function in MMR (Jiricny, 2006).

C. Effect of aphidicolin: alkylated plasmids (pEL97: 11.3kb) were incubated in NPE supplemented or not by aphidicolin (150μM final) in the presence of $^{32}$P-dATP for 1h at RT. Analysis was performed by spot assay as described in Material and Methods. The y-axis represents the percentage of radioactive DNA synthesis expressed in % of full plasmid replication. Addition of Aphidicolin to NPE (150 μM final) more severely reduces incorporation in MNU+, MNU++ and ENU plasmids, compared to control and MMS plasmids. Fold reduction in incorporation under aphidicolin conditions is shown.

**Figure 2-figure supplement 2**. Repair synthesis in HSS extracts.
Plasmid treated with MNU (≈1 N-alkyl adduct/500nt), was incubated in HSS extracts in the presence of α$^{32}$P-dATP; repair synthesis was monitored at room temperature as a function of time using the spot assay. Both DNA0 and MNU plasmids only exhibit background incorporation levels. Robust UDS is observed in MNU-plasmid upon addition of hAAG glycosylase (150nM). Average and standard deviation of two independent experiments.

**Figure 3.** Stimulation of MMR at a single O$^6$mG site by N-alkyl adducts *in cis*.
A. Covalently closed circular (ccc) plasmids (pAS200.2, 2,1 kb) containing a site-specific O$^6$mG:C base pair (plasmid mGC) and the corresponding lesion-free control (plasmid GC) were constructed (Isogawa et al., 2020). Similarly, plasmids with a site specific GT or a O$^6$mG:T mismatch were constructed. All 4 constructs were treated with MMS in order to introduce random N-alkyl (7mG and 3mA) adducts, generating plasmids GC+MMS, mGC+MMS, GT+MMS and mGT+MMS. We adjusted the MMS reaction conditions as to introduce ≈ 9 adducts per plasmid (i.e. one N-alkylation adduct every ≈500 nt). The resulting proportion of O-alk and N-alkyl adducts mimics the proportion in MNU-treated plasmid. The single O$^6$mG adduct and the randomly located N-alkyl adducts are represented by a star and red dots, respectively.
B. Plasmids described above were incubated in NPE supplemented with α$^{32}$P-dATP at room temperature; incorporation of radioactivity was monitored as a function of time using the spot assay. The y-axis represents the percentage of DNA repair synthesis with respect to input DNA (i.e. 10% means that the observed extent of repair synthesis is equivalent to 10% of input plasmid replication). Overall, incorporation into GT and mGT plasmids is higher than incorporation in their GC and mGC counterparts. Incorporation attributable to repair at the O$^6$mG:C lesion is increased close to 3-fold due to the presence of random N-alkyl lesions introduced by MMS treatment. The stimulatory effect of random N-alkyl lesions on GT and mGT repair is observed but is slightly less pronounced than for mGC.
C. The same plasmids were incubated for 2h incubation in NPE, purified, resolved by agarose gel electrophoresis and revealed by ethidium bromide fluorescence and $^{32}$P autoradiography. The total amount of signal per lane is indicated (AU). As expected, the amount of plasmid extracted from each incubation mix is relatively constant, as quantified below the ethidium bromide image. Increase in repair at the O$^6$mG:C lesion due to MMS-treatment (2.8-fold) is in good agreement with data in Figure 3B.

**Figure 3-figure supplement 1**. Mapping repair synthesis in the vicinity of a single O$^6$mG adduct.
A: Agarose gel electrophoresis of the native form of GC, mGC, GC+MMS and mGC+MMS

796 B. Restriction map of pAS201, the two single cutter enzymes *BmtI* and *BaeGI* yield a short S
797 (589bp) and long L (1525bp) fragment, respectively. Fragment S contains the single $O^6$mG
798 adduct.
799 C. Plasmids GC, mGC, GC+MMS and mGC+MMS were incubated in NPE in the presence of
800 $\alpha^{32}$P-dATP and extracted after 2h. The purified plasmids were digested with restriction
801 enzymes *BmtI* and *BaeGI*. Digested plasmids were analyzed by agarose gel electrophoresis
802 and visualized by ethidium bromide staining and by $^{32}$P-imaging.
803 D. The specific activity (SA) of a given fragment (S or L) was quantified as the amount of $^{32}$P
804 incorporated divided by the amount of DNA deduced from the Ethidium bromide
805 fluorescence image (expressed in arbitrary units AU). In control plasmid GC, a similar SA value
806 was observed for both fragments as expected for residual background incorporation;
807 similarly, in MMS treated plasmid (GC + MMS), the SA value is similar for S and L fragments.
808 The slightly increased SA value in GC+MMS compared to GC is compatible with repair
809 synthesis by BER at randomly located MMS-induced lesions. For plasmids containing a single
810 $O^6$mG:C lesion (mGC and mGC+MMS), there is a robust increase in SA of the short compared
811 to the long fragments. Incorporation, above background, due to $O^6$mG, in the absence of
812 MMS, amounts to 0.065 and 0.495 AU for long and short fragments, respectively (signal
813 above dotted line in S3D). Similarly, in the context of MMS lesions, incorporation, above
814 background, due to $O^6$mG amounts to 0.115 and 1,17 AU for long and short fragments,
815 respectively (signal above dotted line in S3D). Taken together these results clearly show that
816 $O^6$mGC-mediated repair specifically takes place in the S fragment, with only modest spill-over
817 into the L fragment (10-15%).
818 E. Plasmid with a single $O^6$mG:C lesion site (mGC) and control plasmid (GC) were incubated in
819 NPE depleted with anti Mlh1 antibodies and mock treated NPE. Incorporation was measured
820 into whole plasmids. The increase in incorporation into mGC compared to GC observed upon
821 incubation in NPE fully disappeared when Mlh1 was depleted. This experiment shows that the
822 increase in incorporation observed in mGC compared to incorporation in control GC plasmid
823 can specifically be attributed to mismatch repair activity at the single $O^6$mG:C lesion
824
825 Figure 4. Double-strand breaks occur in MNU-treated plasmid during incubation in extracts.
826 A. Analysis by AGE of alkylated plasmids (pEL97: 11,3kb) incubated in NPE in the presence of
827 $\alpha^{32}$P-dATP. Plasmid pEL97 was treated with MMS, MNU+ and ENU as to introduce ≈ one
828 alkylation event on average every 500 nt on average. For MNU, a plasmid with twice the level
829 of alkylation (MNU++, 1 lesion every 250 nt) was also produced (Figure 4-figure supplement
830 1). Alkylation of these plasmids essentially not affected their migration on agarose gels (Figure
831 4-figure supplement 2A). After 2h incubation, the reaction was stopped and a known amount
832 of pBR322 (10 ng) plasmid was added as an internal standard. Ethidium bromide image: in the
833 different lanes the internal standard band, pBR (ccc), appears to be of similar intensity (1158
834 +/- 95 AU), assessing reproducible DNA extraction. For the alkylated plasmids, incubation in
835 NPE led to massive conversion from ccc to relaxed plasmid. $^{32}$P image: Little incorporation of
836 $^{32}$P-dATP is seen in DNA0 and in MMS-treated plasmid compared to MNU and ENU treated
837 plasmids as shown by the relative incorporation levels normalized to 1 for untreated plasmid
838 (DNA0). As expected, the MNU++ sample exhibits about twice the amount of incorporated
839 radioactivity compared to MNU+. In both Ethidium bromide and $^{32}$P images, a small amount
840 of linear plasmid is seen mostly in the MNU++ sample. This band is also visible in the MNU+
841 and ENU lanes although at a weaker intensity.

842 B. Quadratic dose-response for DSB formation. When the % of linear form (linear/(linear +
843 oc)), is plotted as a function of the square dose of MNU ($mM^2$) for untreated, MNU+ and
844 MNU++ plasmids, we observed a straight line (y = 1,4173x - 0,0288; $R^2$ = 0,9999).
845
846 Figure 4-figure supplement 1. Estimation of N-alkylation levels of modification by MMS and
847 MNU.
848 A. Alkaline fragmentation of alkylated plasmid (pEL97, 11.3 kb) DNA is analyzed by agarose gel
849 electrophoresis. B. Densitometry of the ethidium bromide-stained agarose gel. C. Estimation
850 of the average number of alkali cleavage sites per plasmid strand. The data reveal that the
851 average number of cleavage sites per plasmid strand is 21-23 for both MMS and MNU+
852 reaction conditions (the average distance between two sites is ≈ 510 nt). For MNU++, the
853 average distance between two cleavage sites is ≈254 nt.
854
855 Figure 4-figure supplement 2. Fragmentation of alkylated plasmid as analyzed on AGE loaded
856 under alkaline conditions.
857 A: Alkylation did not affect plasmids topology except for ENU treatment that increases
858 relaxation as seen in the AGE image.
859 B: Analysis by AGE, under alkaline loading conditions, of alkylated plasmids (pEL97: 11,3kb)
860 incubated in NPE in the presence of $\alpha^{32}$P-dATP (same samples as in Figure 4A). Loading under
861 alkaline conditions allowed single-stranded nicks to be revealed. In the different lanes, an
862 internal standard band, pBR (ccc), was introduced before the extraction procedure in order to
863 assess consistent recovery of DNA during extraction (as seen by ethidium bromide staining).
864 For the alkylated plasmids, incubation in NPE led to massive conversion of plasmid DNA into a
865 smear with a low amount of DNA present as a single-stranded linear band (doublet). For the
866 MNU++ sample, no linear ss DNA was seen, all DNA was converted into a smear. The
867 smearing can best be seen in the $^{32}$P image. We suggest that the ss DNA fragments that form
868 the smear arise between a gap caused by a MMR event at a $O^6$mG sites and an uncompleted
869 BER event at a neighbor lesion. It cannot be excluded that some fragments result from MMR
870 attempts at two $O^6$mG lesions. The intense $^{32}$P labelling of the fragments in the smear result
871 from incorporation of up to several hundred nt during a single MMR repair synthesis.
872 Relative $^{32}$P incorporation normalized to 1 for DNA0 are indicated below the $^{32}$P-image.
873
874 Figure 5: Simultaneous repair of two closely spaced MNU-induced lesions may lead to a DSB.
875 Such a situation occurs when an N-alkyl lesion located within ≈500nt of an $O^6$mG lesion are
876 processed simultaneously ("Lesion Arrangement at-risk"). Note that the MMR excision track
877 can occur on either strand as described for noncanonical MMR (Peña-Diaz et al., 2012).
878 Reaction of MNU with double-stranded DNA induces N-alkylation adducts, mostly 7mG and
879 3mA shown as * and O-alkylation adducts ($O^6$mG), at a 10:1 ratio approximatively. Step 1: a
880 BER event is initiated at an N-alkyl adduct, creating a nick. Step 2: concomitantly, a MMR
881 event takes place, in the opposite strand, at a nearby at a $O^6$mG:C site. Step 3: the MMR
882 machinery extends the nick into a several hundred nt long gap by means of Exo1 action. Step
883 4: The two independently initiated repair events lead to a DSB, if the MMR gap reaches the
884 BER initiated nick before resealing.
885
886
887
888

889

890

891 References:

892

893 Aas, P.A., Otterlei, M., Falnes, P.O., Vågbø, C.B., Skorpen, F., Akbari, M., Sundheim, O., Bjørås,
894 M., Slupphaug, G., Seeberg, E., Krokan, H.E., 2003. Human and bacterial oxidative
895 demethylases repair alkylation damage in both RNA and DNA. Nature 421, 859–863.
896 doi:10.1038/nature01363
897 Baranovskiy, A.G., Babayeva, N.D., Suwa, Y., Gu, J., Pavlov, Y.I., Tahirov, T.H., 2014. Structural
898 basis for inhibition of DNA replication by aphidicolin. Nucleic Acids Res 42, 14013–14021.
899 doi:10.1093/nar/gku1209
900 Beranek, D.T., 1990. Distribution of methyl and ethyl adducts following alkylation with
901 monofunctional alkylating agents. Mutat Res 231, 11–30.
902 Bhanot, O.S., Ray, A., 1986. The in vivo mutagenic frequency and specificity of O6-
903 methylguanine in phi X174 replicative form DNA. Proc Natl Acad Sci USA 83, 7348–7352.
904 doi:10.1073/pnas.83.19.7348
905 Bobola, M.S., Kolstoe, D.D., Blank, A., Silber, J.R., 2010. Minimally cytotoxic doses of
906 temozolomide produce radiosensitization in human glioblastoma cells regardless of
907 MGMT expression. Mol. Cancer Ther. 9, 1208–1218. doi:10.1158/1535-7163.MCT-10-
908 0010
909 Bregenhorn, S., Kallenberger, L., Artola-Borán, M., Peña-Diaz, J., Jiricny, J., 2016. Non-
910 canonical uracil processing in DNA gives rise to double-strand breaks and deletions:
911 relevance to class switch recombination. Nucleic Acids Res 44, 2691–2705.
912 doi:10.1093/nar/gkv1535
913 Cejka, P., Jiricny, J., 2008. Interplay of DNA repair pathways controls methylation damage
914 toxicity in Saccharomyces cerevisiae. Genetics 179, 1835–1844.
915 doi:10.1534/genetics.108.089979
916 Chakravarti, D., Ibeanu, G.C., Tano, K., Mitra, S., 1991. Cloning and expression in Escherichia
917 coli of a human cDNA encoding the DNA repair protein N-methylpurine-DNA glycosylase.
918 J Biol Chem 266, 15710–15715.
919 Day, R.S., Ziolkowski, C.H., Scudiero, D.A., Meyer, S.A., Lubiniecki, A.S., Girardi, A.J., Galloway,
920 S.M., Bynum, G.D., 1980. Defective repair of alkylated DNA by human tumour and SV40-
921 transformed human cell strains. Nature 288, 724–727. doi:10.1038/288724a0
922 Demple, B., Jacobsson, A., Olsson, M., Robins, P., Lindahl, T., 1982. Repair of alkylated DNA in
923 Escherichia coli. Physical properties of O6-methylguanine-DNA methyltransferase. J Biol
924 Chem 257, 13776–13780.
925 Duckett, D.R., Bronstein, S.M., Taya, Y., Modrich, P., 1999. hMutSalpha- and hMutLalpha-
926 dependent phosphorylation of p53 in response to DNA methylator damage. Proc Natl
927 Acad Sci USA 96, 12384–12388. doi:10.1073/pnas.96.22.12384
928 Duncan, T., Trewick, S.C., Koivisto, P., Bates, P.A., Lindahl, T., Sedgwick, B., 2002. Reversal of
929 DNA alkylation damage by two human dioxygenases. Proc Natl Acad Sci USA 99, 16660–
930 16665. doi:10.1073/pnas.262589799
931 Elias, J.E., Gygi, S.P., 2010. Target-decoy search strategy for mass spectrometry-based
932 proteomics. Methods Mol. Biol. 604, 55–71. doi:10.1007/978-1-60761-444-9_5
933 Elias, J.E., Gygi, S.P., 2007. Target-decoy search strategy for increased confidence in large-
934 scale protein identifications by mass spectrometry. Nat. Methods 4, 207–214.
935 doi:10.1038/nmeth1019

936 Ensminger, M., Iloff, L., Ebel, C., Nikolova, T., Kaina, B., Löbrich, M., 2014. DNA breaks and
937 chromosomal aberrations arise when replication meets base excision repair. J. Cell Biol.
938 206, 29–43. doi:10.1083/jcb.201312078
939 Falnes, P.O., Johansen, R.F., Seeberg, E., 2002. AlkB-mediated oxidative demethylation
940 reverses DNA damage in Escherichia coli. Nature 419, 178–182. doi:10.1038/nature01048
941 Goldmacher, V.S., Cuzick, R.A., Thilly, W.G., 1986. Isolation and partial characterization of
942 human cell mutants differing in sensitivity to killing and mutation by methylnitrosourea
943 and N-methyl-N'-nitro-N-nitrosoguanidine. J Biol Chem 261, 12462–12471.
944 Graham, T.G.W., Walter, J.C., Loparo, J.J., 2016. Two-Stage Synapsis of DNA Ends during Non-
945 homologous End Joining. Mol Cell 61, 850–858. doi:10.1016/j.molcel.2016.02.010
946 Gupta, D., Heinen, C.D., 2019. The mismatch repair-dependent DNA damage response:
947 Mechanisms and implications. DNA Repair (Amst) 78, 60–69.
948 doi:10.1016/j.dnarep.2019.03.009
949 Huttlin, E.L., Bruckner, R.J., Paulo, J.A., Cannon, J.R., Ting, L., Baltier, K., Colby, G., Gebreab, F.,
950 Gygi, M.P., Parzen, H., Szpyt, J., Tam, S., Zarraga, G., Pontano-Vaites, L., Swarup, S., White,
951 A.E., Schweppe, D.K., Rad, R., Erickson, B.K., Obar, R.A., Guruharsha, K.G., Li, K., Artavanis-
952 Tsakonas, S., Gygi, S.P., Harper, J.W., 2017. Architecture of the human interactome
953 defines protein communities and disease networks. Nature. doi:10.1038/nature22366
954 Isogawa, A., Fuchs, R.P., Fujii, S., 2020. Chromatin Pull-Down Methodology Based on DNA
955 Triple Helix Formation. Methods Mol. Biol. 2119, 183–199. doi:10.1007/978-1-0716-
956 0323-9_16
957 Isogawa, A., Fuchs, R.P., Fujii, S., 2018. Versatile and efficient chromatin pull-down
958 methodology based on DNA triple helix formation. Sci Rep 8, 5925. doi:10.1038/s41598-
959 018-24417-9
960 Jiricny, J., 2006. The multifaceted mismatch-repair system. Nat Rev Mol Cell Biol 7, 335–346.
961 doi:10.1038/nrm1907
962 Kaina, B., Christmann, M., 2019. Corrigendum to “DNA repair in personalized brain cancer
963 therapy with temozolomide and nitrosoureas” [DNA Repair 78 (2019) 128-141]. DNA
964 Repair (Amst) 80, 93. doi:10.1016/j.dnarep.2019.06.003
965 Kaina, B., Christmann, M., Naumann, S., Roos, W.P., 2007. MGMT: key node in the battle
966 against genotoxicity, carcinogenicity and apoptosis induced by alkylating agents. DNA
967 Repair (Amst) 6, 1079–1099. doi:10.1016/j.dnarep.2007.03.008
968 Karran, P., 2001. Mechanisms of tolerance to DNA damaging therapeutic drugs.
969 Carcinogenesis 22, 1931–1937. doi:10.1093/carcin/22.12.1931
970 Karran, P., Bignami, M., 1994. DNA damage tolerance, mismatch repair and genome
971 instability. Bioessays 16, 833–839. doi:10.1002/bies.950161110
972 Karran, P., Macpherson, P., Ceccotti, S., Dogliotti, E., Griffin, S., Bignami, M., 1993. O6-
973 methylguanine residues elicit DNA repair synthesis by human cell extracts. J Biol Chem
974 268, 15878–15886.
975 Karran, P., Marinus, M.G., 1982. Mismatch correction at O6-methylguanine residues in E. coli
976 DNA. Nature 296, 868–869. doi:10.1038/296868a0
977 Kat, A., Thilly, W.G., Fang, W.H., Longley, M.J., Li, G.M., Modrich, P., 1993. An alkylation-
978 tolerant, mutator human cell line is deficient in strand-specific mismatch repair. Proc Natl
979 Acad Sci USA 90, 6424–6428.
980 Kato, N., Kawasoe, Y., Williams, H., Coates, E., Roy, U., Shi, Y., Beese, L.S., Schärer, O.D., Yan,
981 H., Gottesman, M.E., Takahashi, T.S., Gautier, J., 2017. Sensing and Processing of DNA

Interstrand Crosslinks by the Mismatch Repair Pathway. Cell Rep 21, 1375–1385. doi:10.1016/j.celrep.2017.10.032

Kawasoe, Y., Tsurimoto, T., Nakagawa, T., Masukata, H., Takahashi, T.S., 2016. MutSα maintains the mismatch repair capability by inhibiting PCNA unloading. Elife 5. doi:10.7554/eLife.15155

Lebofsky, R., Takahashi, T., Walter, J.C., 2009. DNA replication in nucleus-free Xenopus egg extracts. Methods Mol. Biol. 521, 229–252. doi:10.1007/978-1-60327-815-7_13

Lindahl, T., 1976. New class of enzymes acting on damaged DNA. Nature 259, 64–66. doi:10.1038/259064a0

Liu, Y., Fang, Y., Shao, H., Lindsey-Boltz, L., Sancar, A., Modrich, P., 2010. Interactions of human mismatch repair proteins MutSalpha and MutLalpha with proteins of the ATR-Chk1 pathway. J Biol Chem 285, 5974–5982. doi:10.1074/jbc.M109.076109

Loechler, E.L., 1994. A violation of the Swain-Scott principle, and not SN1 versus SN2 reaction mechanisms, explains why carcinogenic alkylating agents can form different proportions of adducts at oxygen versus nitrogen in DNA. Chem. Res. Toxicol. 7, 277–280. doi:10.1021/tx00039a001

Loechler, E.L., Green, C.L., Essigmann, J.M., 1984. In vivo mutagenesis by O6-methylguanine built into a unique site in a viral genome. Proc Natl Acad Sci USA 81, 6271–6275. doi:10.1073/pnas.81.20.6271

Maxam, A.M., Gilbert, W., 1977. A new method for sequencing DNA. Proc Natl Acad Sci USA 74, 560–564.

Mazon, G., Philippin, G., Cadet, J., Gasparutto, D., Modesti, M., Fuchs, R.P., 2010. Alkyltransferase-like protein (eATL) prevents mismatch repair-mediated toxicity induced by O6-alkylguanine adducts in Escherichia coli. Proc. Natl. Acad. Sci. U.S.A. 107, 18050–18055. doi:10.1073/pnas.1008635107

Meira, L.B., Moroski-Erkul, C.A., Green, S.L., Calvo, J.A., Bronson, R.T., Shah, D., Samson, L.D., 2009. Aag-initiated base excision repair drives alkylation-induced retinal degeneration in mice. Proc Natl Acad Sci USA 106, 888–893. doi:10.1073/pnas.0807030106

Moody, C.L., Wheelhouse, R.T., 2014. The medicinal chemistry of imidazotetrazine prodrugs. Pharmaceuticals (Basel) 7, 797–838. doi:10.3390/ph7070797

Nagatsugi, F., Sasaki, S., Miller, P.S., Seidman, M.M., 2003. Site-specific mutagenesis by triple helix-forming oligonucleotides containing a reactive nucleoside analog. Nucleic Acids Res 31, e31–31. doi:10.1093/nar/gng031

Noonan, E.M., Shah, D., Yaffe, M.B., Lauffenburger, D.A., Samson, L.D., 2012. O6-Methylguanine DNA lesions induce an intra-S-phase arrest from which cells exit into apoptosis governed by early and late multi-pathway signaling network activation. Integr Biol (Camb) 4, 1237–1255. doi:10.1039/c2ib20091k

Nowosielska, A., Marinus, M.G., 2008. DNA mismatch repair-induced double-strand breaks. DNA Repair (Amst) 7, 48–56. doi:10.1016/j.dnarep.2007.07.015

Ochs, K., Kaina, B., 2000. Apoptosis induced by DNA damage O6-methylguanine is Bcl-2 and caspase-9/3 regulated and Fas/caspase-8 independent. Cancer Res 60, 5815–5824.

Olivera Harris, M., Kallenberger, L., Artola-Borán, M., Enoiu, M., Costanzo, V., Jiricny, J., 2015. Mismatch repair-dependent metabolism of O(6)-methylguanine-containing DNA in Xenopus laevis egg extracts. DNA Repair (Amst) 28C, 1–7. doi:10.1016/j.dnarep.2015.01.014

1027 Olsson, M., Lindahl, T., 1980. Repair of alkylated DNA in Escherichia coli. Methyl group
1028 transfer from O6-methylguanine to a protein cysteine residue. J Biol Chem 255, 10569–
1029 10571.
1030 Ortega, J., Lee, G.S., Gu, L., Yang, W., Li, G.-M., 2021. Mispair-bound human MutS-MutL
1031 complex triggers DNA incisions and activates mismatch repair. Cell Res. 31, 542–553.
1032 doi:10.1038/s41422-021-00468-y
1033 Peña-Diaz, J., Bregenhorn, S., Ghodgaonkar, M., Follonier, C., Artola-Borán, M., Castor, D.,
1034 Lopes, M., Sartori, A.A., Jiricny, J., 2012. Noncanonical mismatch repair as a source of
1035 genomic instability in human cells. Mol Cell 47, 669–680.
1036 doi:10.1016/j.molcel.2012.07.006
1037 Plant, J.E., Roberts, J.J., 1971. A novel mechanism for the inhibition of DNA synthesis following
1038 methylation: the effect of N-methyl-N-nitrosourea on HeLa cells. Chem. Biol. Interact. 3,
1039 337–342.
1040 Pluciennik, A., Burdett, V., Baitinger, C., Iyer, R.R., Shi, K., Modrich, P., 2013. Extrahelical
1041 (CAG)/(CTG) triplet repeat elements support proliferating cell nuclear antigen loading and
1042 MutLα endonuclease activation. Proc. Natl. Acad. Sci. U.S.A. 110, 12277–12282.
1043 doi:10.1073/pnas.1311325110
1044 Pluciennik, A., Dzantiev, L., Iyer, R.R., Constantin, N., Kadyrov, F.A., Modrich, P., 2010. PCNA
1045 function in the activation and strand direction of MutLα endonuclease in mismatch
1046 repair. Proc. Natl. Acad. Sci. U.S.A. 107, 16066–16071. doi:10.1073/pnas.1010662107
1047 Quiros, S., Roos, W.P., Kaina, B., 2010. Processing of O6-methylguanine into DNA double-
1048 strand breaks requires two rounds of replication whereas apoptosis is also induced in
1049 subsequent cell cycles. Cell Cycle 9, 168–178. doi:10.4161/cc.9.1.10363
1050 Repmann, S., Olivera Harris, M., Jiricny, J., 2015. Influence of oxidized purine processing on
1051 strand directionality of mismatch repair. J Biol Chem 290, 9986–9999.
1052 doi:10.1074/jbc.M114.629907
1053 Sattler, U., Frit, P., Salles, B., Calsou, P., 2003. Long-patch DNA repair synthesis during base
1054 excision repair in mammalian cells. EMBO Rep. 4, 363–367.
1055 doi:10.1038/sj.embor.embor796
1056 Schanz, S., Castor, D., Fischer, F., Jiricny, J., 2009. Interference of mismatch and base excision
1057 repair during the processing of adjacent U/G mispairs may play a key role in somatic
1058 hypermutation. Proc. Natl. Acad. Sci. U.S.A. 106, 5593–5598.
1059 doi:10.1073/pnas.0901726106
1060 Simonelli, V., Leuzzi, G., Basile, G., D'Errico, M., Fortini, P., Franchitto, A., Viti, V., Brown, A.R.,
1061 Parlanti, E., Pascucci, B., Palli, D., Giuliani, A., Palombo, F., Sobol, R.W., Dogliotti, E., 2017.
1062 Crosstalk between mismatch repair and base excision repair in human gastric cancer.
1063 Oncotarget 8, 84827–84840. doi:10.18632/oncotarget.10185
1064 Strobel, H., Baisch, T., Fitzel, R., Schilberg, K., Siegelin, M.D., Karpel-Massler, G., Debatin, K.-
1065 M., Westhoff, M.-A., 2019. Temozolomide and Other Alkylating Agents in Glioblastoma
1066 Therapy. Biomedicines 7, 69. doi:10.3390/biomedicines7030069
1067 Tang, J.-B., Svilar, D., Trivedi, R.N., Wang, X.-H., Goellner, E.M., Moore, B., Hamilton, R.L.,
1068 Banze, L.A., Brown, A.R., Sobol, R.W., 2011. N-methylpurine DNA glycosylase and DNA
1069 polymerase beta modulate BER inhibitor potentiation of glioma cells to temozolomide.
1070 Neuro-oncology 13, 471–486. doi:10.1093/neuonc/nor011
1071 Tano, K., Shiota, S., Collier, J., Foote, R.S., Mitra, S., 1990. Isolation and structural
1072 characterization of a cDNA clone encoding the human DNA repair protein for O6-
1073 alkylguanine. Proc Natl Acad Sci USA 87, 686–690. doi:10.1073/pnas.87.2.686

Trewick, S.C., Henshaw, T.F., Hausinger, R.P., Lindahl, T., Sedgwick, B., 2002. Oxidative demethylation by Escherichia coli AlkB directly reverts DNA base damage. Nature 419, 174–178. doi:10.1038/nature00908

Trivedi, R.N., Almeida, K.H., Fornsaglio, J.L., Schamus, S., Sobol, R.W., 2005. The Role of Base Excision Repair in the Sensitivity and Resistance to Temozolomide-Mediated Cell Death. Cancer Res 65, 6394–6400. doi:10.1158/0008-5472.CAN-05-0715

Walter, J., Sun, L., Newport, J., 1998. Regulated chromosomal DNA replication in the absence of a nucleus. Mol Cell 1, 519–529. doi:10.1016/s1097-2765(00)80052-0

Wühr, M., Freeman, R.M., Presler, M., Horb, M.E., Peshkin, L., Gygi, S.P., Kirschner, M.W., 2014. Deep proteomics of the Xenopus laevis egg using an mRNA-derived reference database. Curr. Biol. 24, 1467–1475. doi:10.1016/j.cub.2014.05.044

Yarosh, D.B., Foote, R.S., Mitra, S., Day, R.S., 1983. Repair of O6-methylguanine in DNA by demethylation is lacking in Mer- human tumor cell strains. Carcinogenesis 4, 199–205. doi:10.1093/carcin/4.2.199

York, S.J., Modrich, P., 2006. Mismatch repair-dependent iterative excision at irreparable O6-methylguanine lesions in human nuclear extracts. J Biol Chem 281, 22674–22683. doi:10.1074/jbc.M603667200

Yoshioka, K.-I., Yoshioka, Y., Hsieh, P., 2006. ATR kinase activation mediated by MutSalpha and MutLalpha in response to cytotoxic O6-methylguanine adducts. Mol Cell 22, 501–510. doi:10.1016/j.molcel.2006.04.023

Zlatanou, A., Despras, E., Braz-Petta, T., Boubakour-Azzouz, I., Pouvelle, C., Stewart, G.S., Nakajima, S., Yasui, A., Ishchenko, A.A., Kannouche, P.L., 2011. The hMsh2-hMsh6 Complex Acts in Concert with Monoubiquitinated PCNA and Pol η in Response to Oxidative DNA Damage in Human Cells. Mol Cell 43, 649–662. doi:10.1016/j.molcel.2011.06.023

A

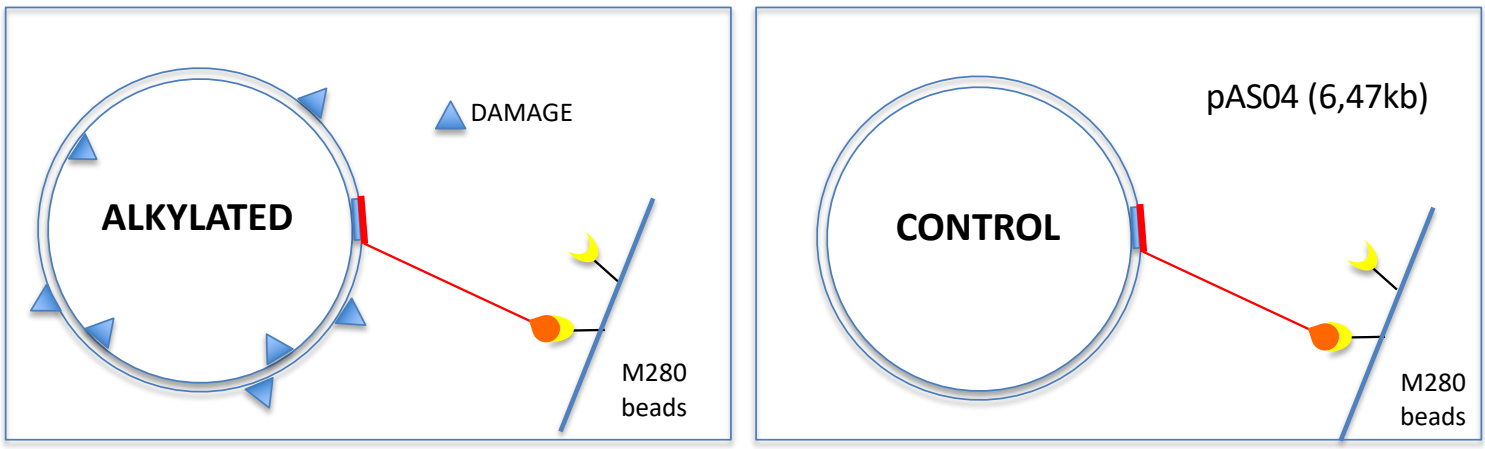
ALKYLATED
DAMAGE
M280
beads
CONTROL
pAS04 (6,47kb)
M280
beads

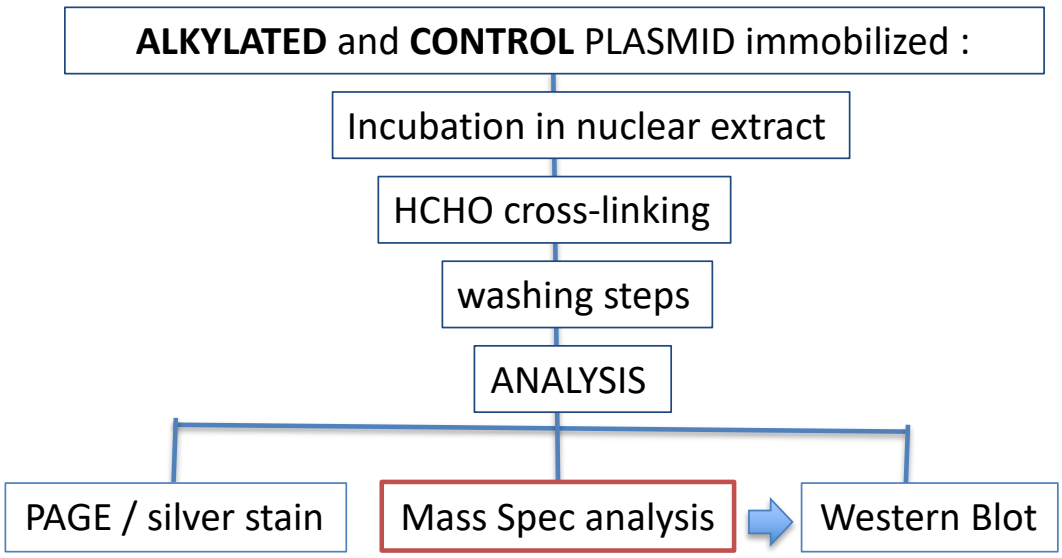
ALKYLATED and CONTROL PLASMID immobilized :
Incubation in nuclear extract
HCHO cross-linking
washing steps
ANALYSIS
PAGE / silver stain
Mass Spec analysis
Western Blot

B

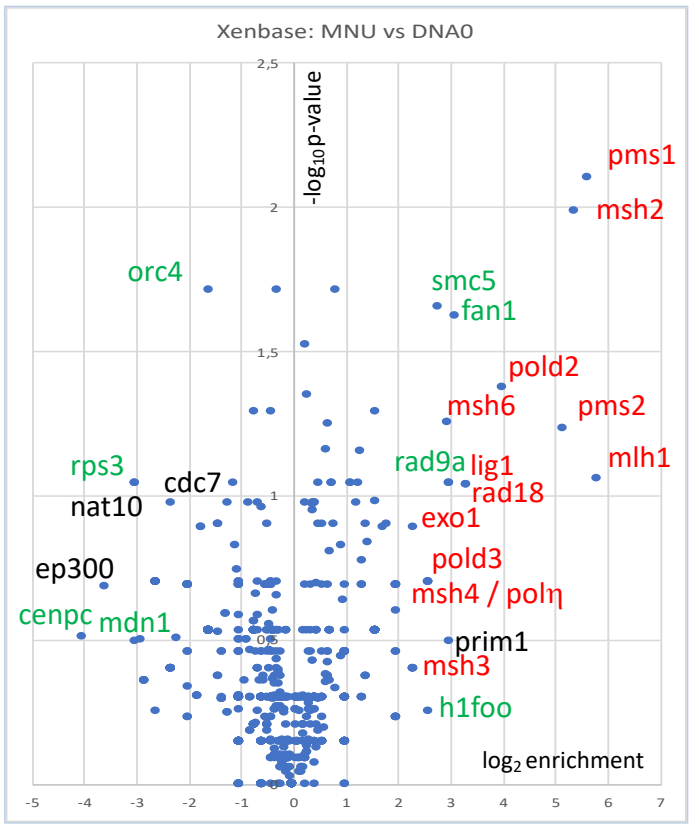
Xenbase: MNU vs DNA0
-log10 p-value
log2 enrichment
pms1
msh2
orc4
smc5
fan1
pold2
msh6
pms2
mlh1
rps3
cdc7
nat10
rad9a
lig1
rad18
exo1
pold3
ep300
msh4 / polη
cenpc
mdn1
prim1
msh3
h1foo

C

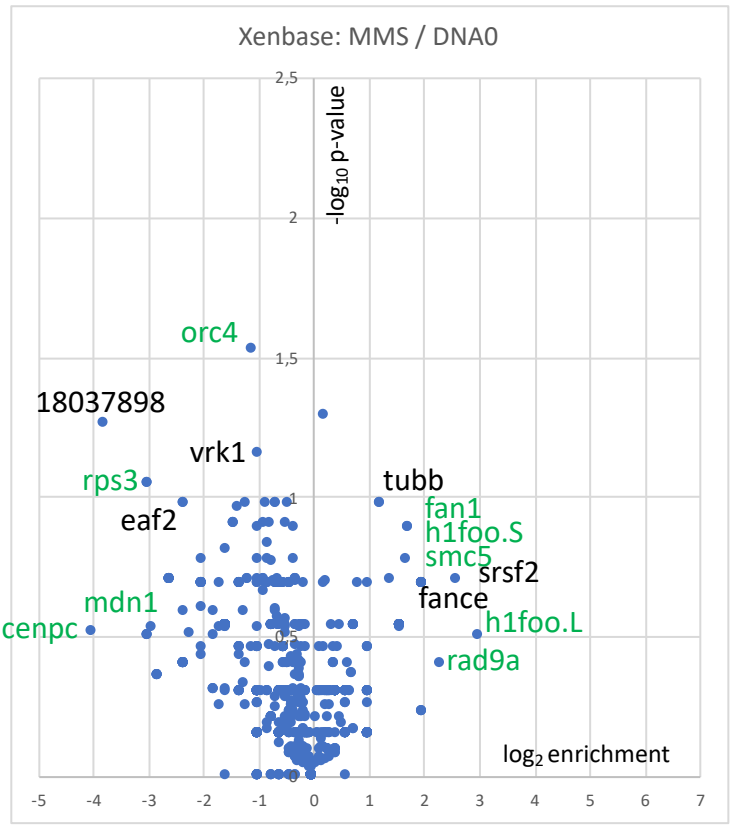
Xenbase: MMS / DNA0
-log10 p-value
log2 enrichment
orc4
18037898
vrk1
rps3
tubb
eaf2
fan1
h1foo.S
smc5
srsf2
fance
mdn1
cenpc
h1foo.L
rad9a

Figure 1

A.

| 0.65 ml tube | DNA0 | MMS: 10mM final | MNU: 1mM final | ENU: 30mM final |
|---|---|---|---|---|
| pBR322 1ug in CE buffer | 90ul | 90ul | 90ul | 90ul |
| Alkylating agent in DMSO | 10ul DMSO | 10ul MMS at 100mM | 10ul MNU at 10mM | 10ul ENU at 300mM |
| Temp / time | 50°C / 40 min | 40°C / 30min | 50°C / 16 min | 50°C / 40 min |

Alkylation reaction conditions leading to an average of one N- alkylation adduct every 500 nt.

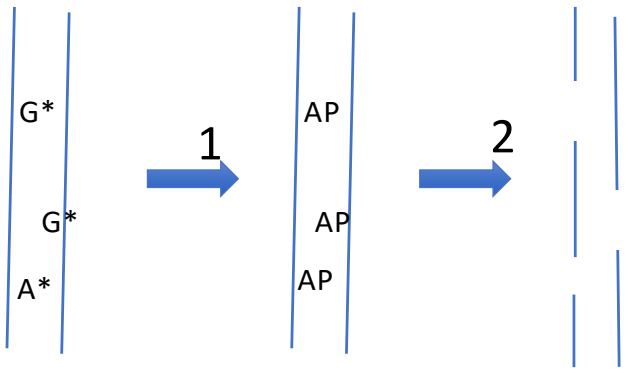


Cleavage at 7mG (G*) and 3mA adducts (A*):
1. Heat-induced depurination at pH7 (90°C, 15')
2. Heat-induced strand cleavage at pH13 (90°C, 30')

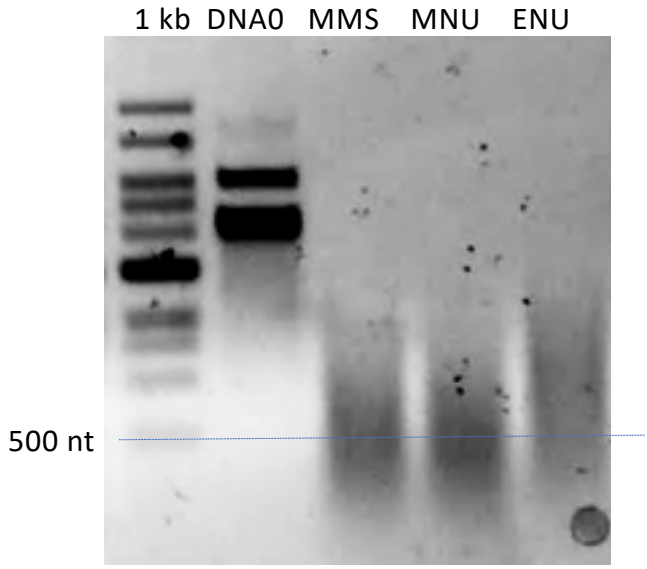


B.

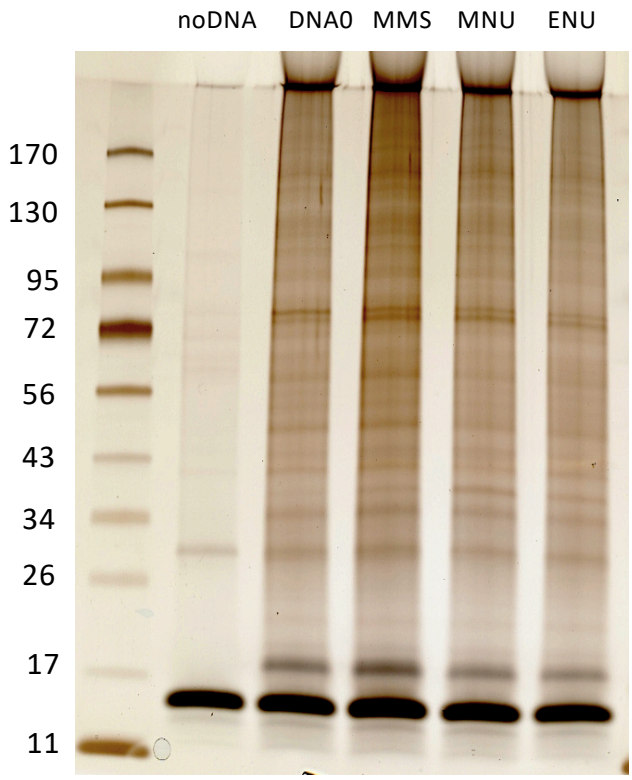


C.

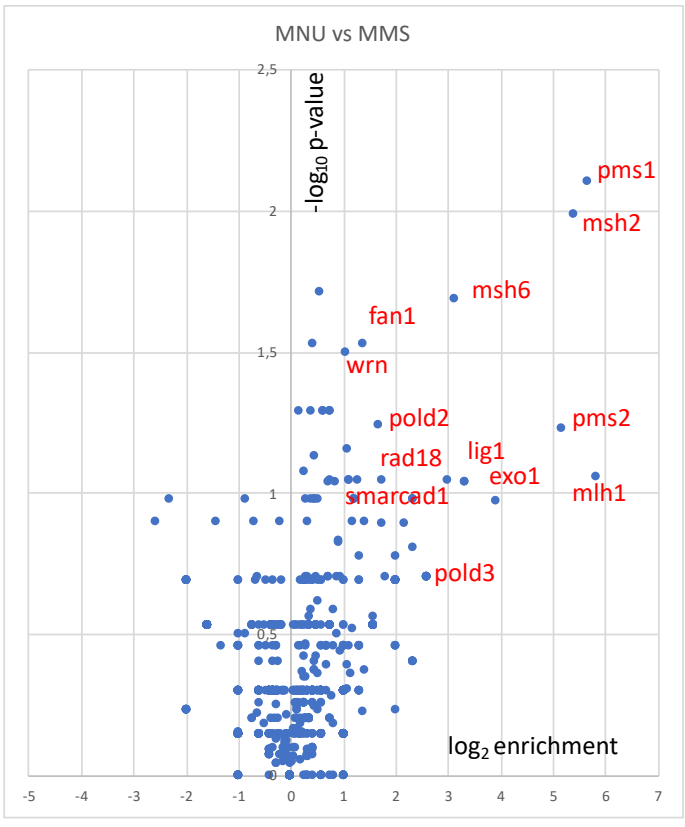


Figure 1-figure supplement 1

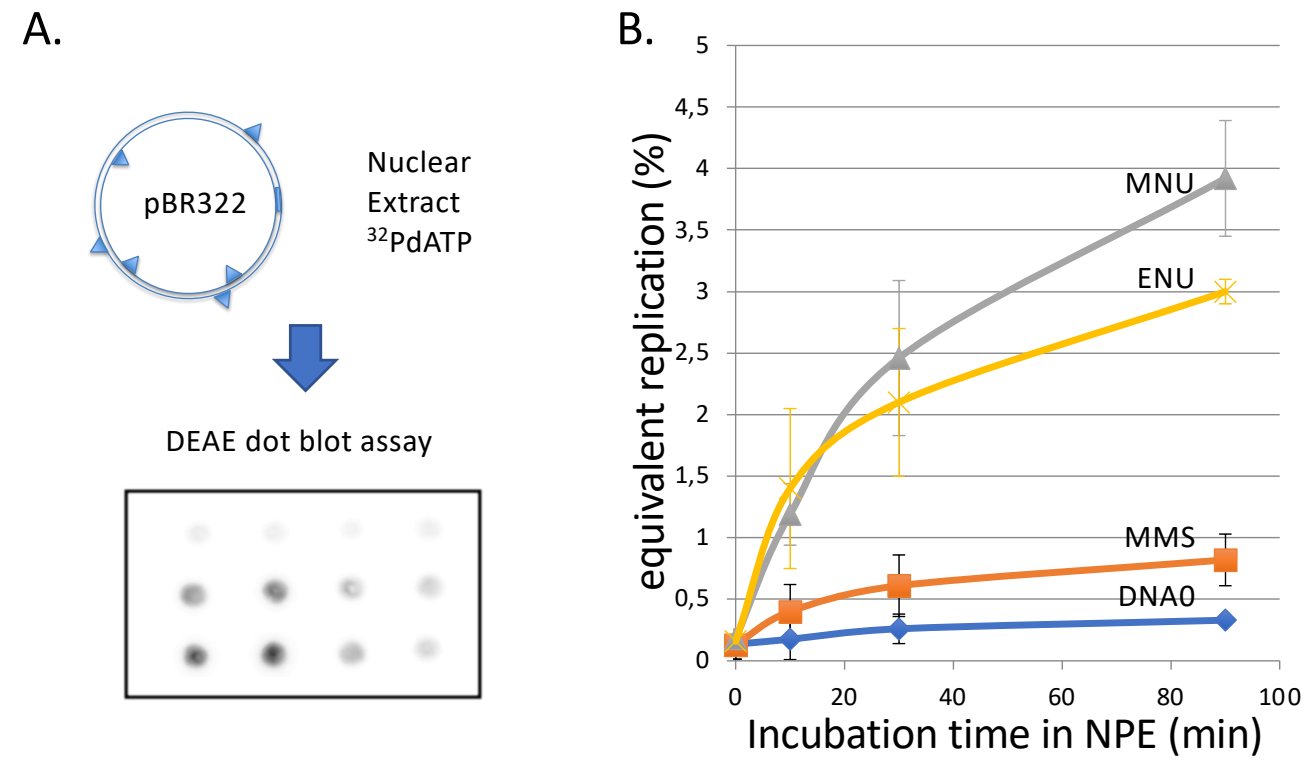
A.
pBR322
Nuclear
Extract
32PdATP
DEAE dot blot assay
B.
equivalent replication (%)
Incubation time in NPE (min)
MNU
ENU
MMS
DNA0
0
0,5
1
1,5
2
2,5
3
3,5
4
4,5
5
0
20
40
60
80
100

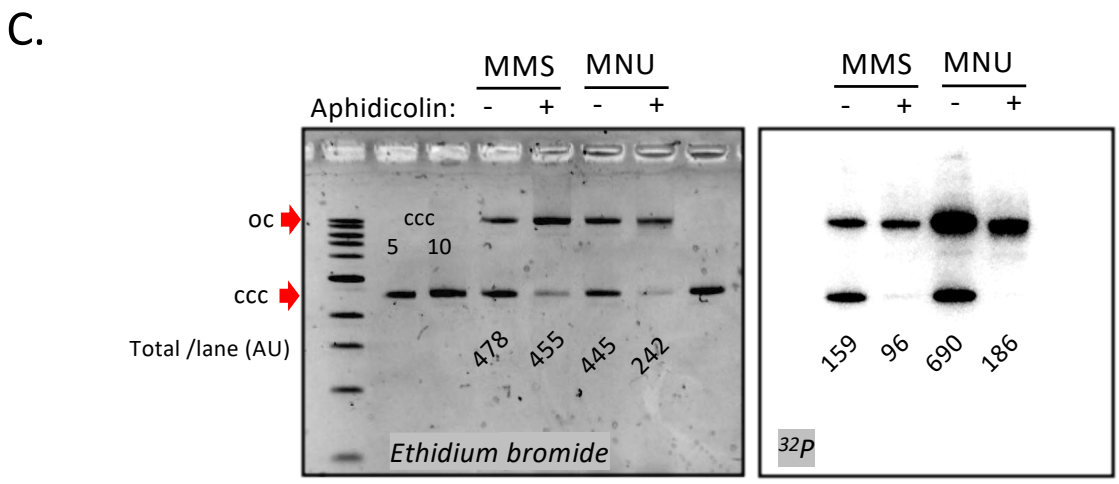
C.
MMS
MNU
Aphidicolin:
- + - +
oc
ccc
Total /lane (AU)
5 10
478
455
445
242
Ethidium bromide
159
96
690
186
32P

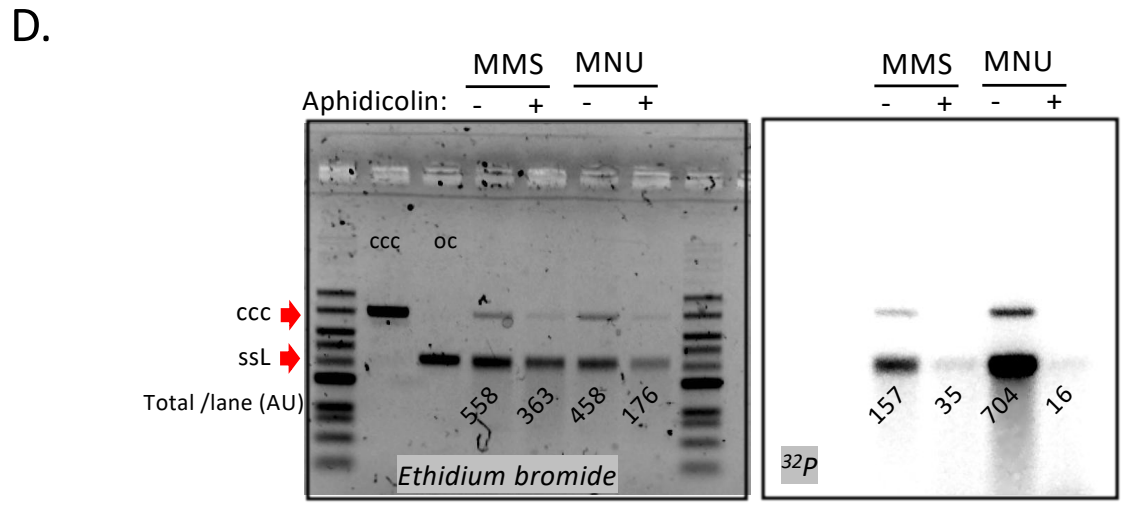
D.
MMS
MNU
Aphidicolin:
- + - +
ccc
oc
ccc
ssL
Total /lane (AU)
558
363
458
176
Ethidium bromide
157
35
704
16
32P

Figure 2

A.

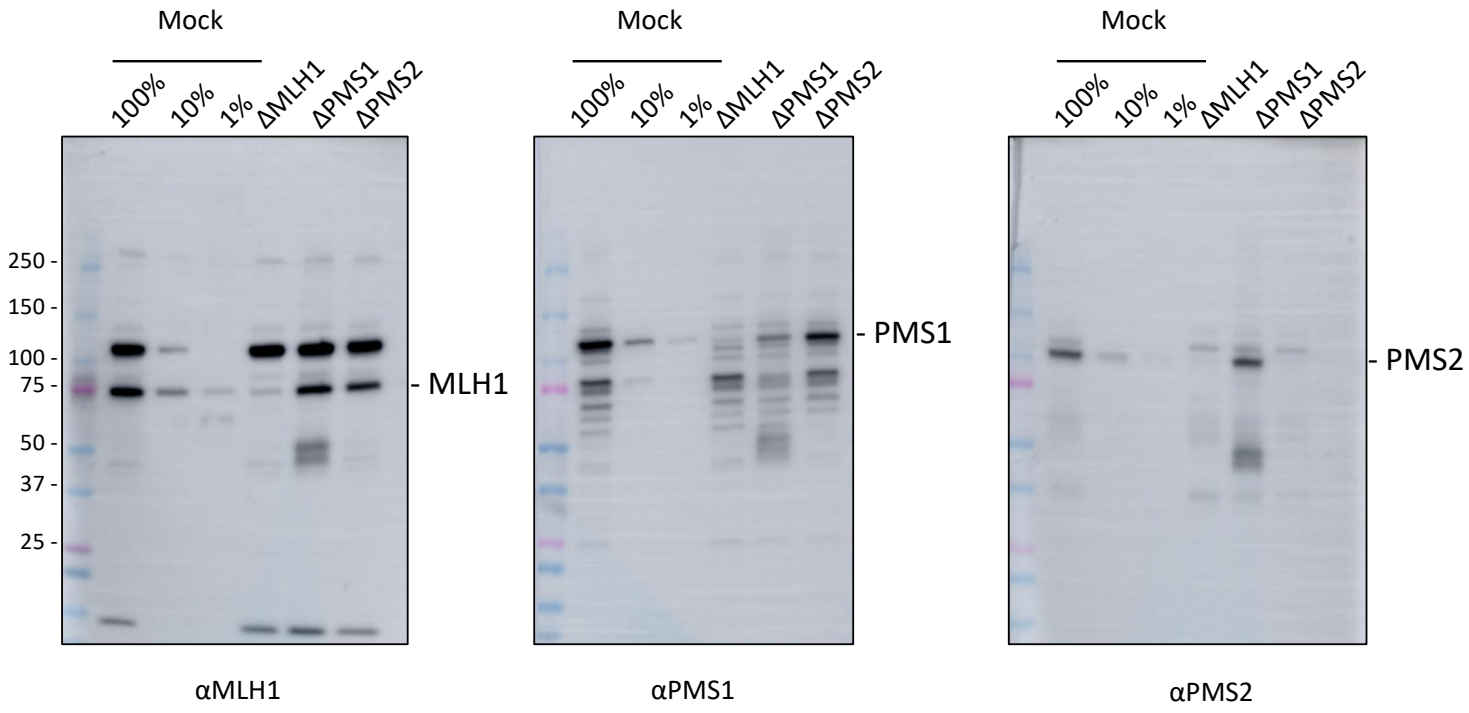


B.

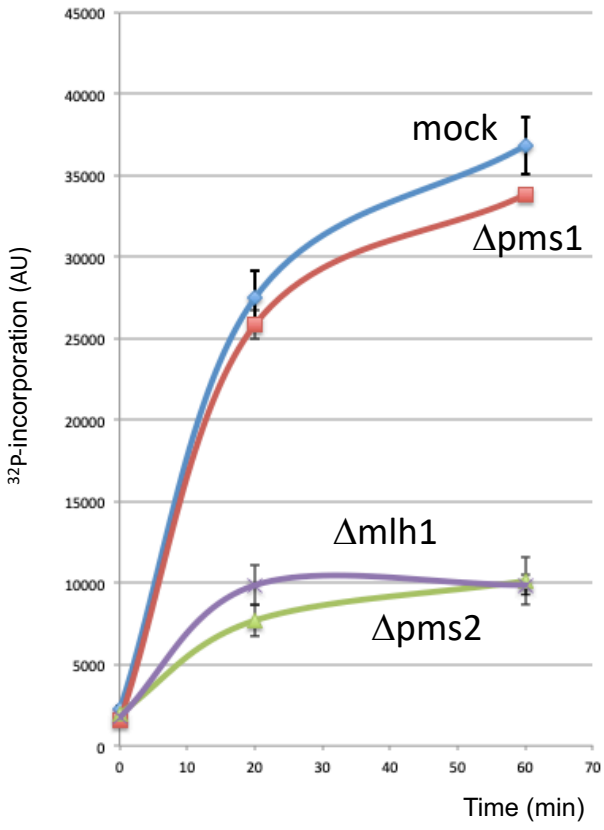


C.

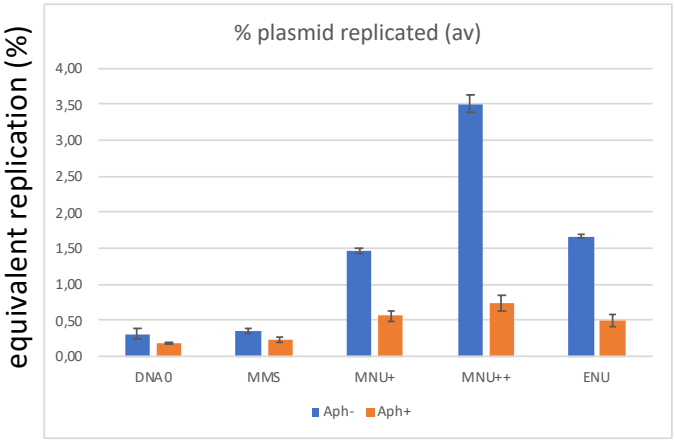


| fold-reduction due to +Aph | 1.6 | 1.4 | 2.6 | 4.8 | 3.3 |
|---|---|---|---|---|---|

Figure 2-figure supplement 1

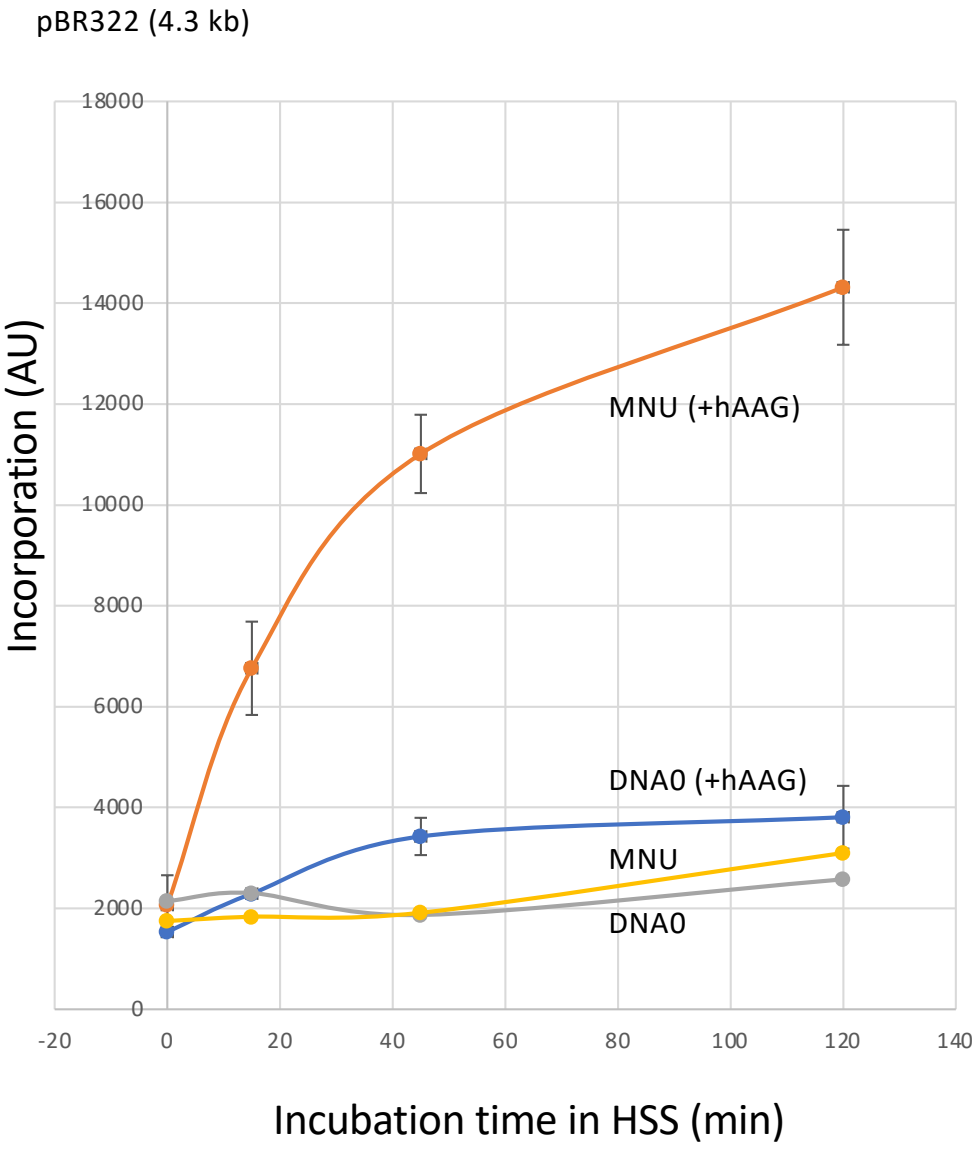


Figure 2-figure supplement 2

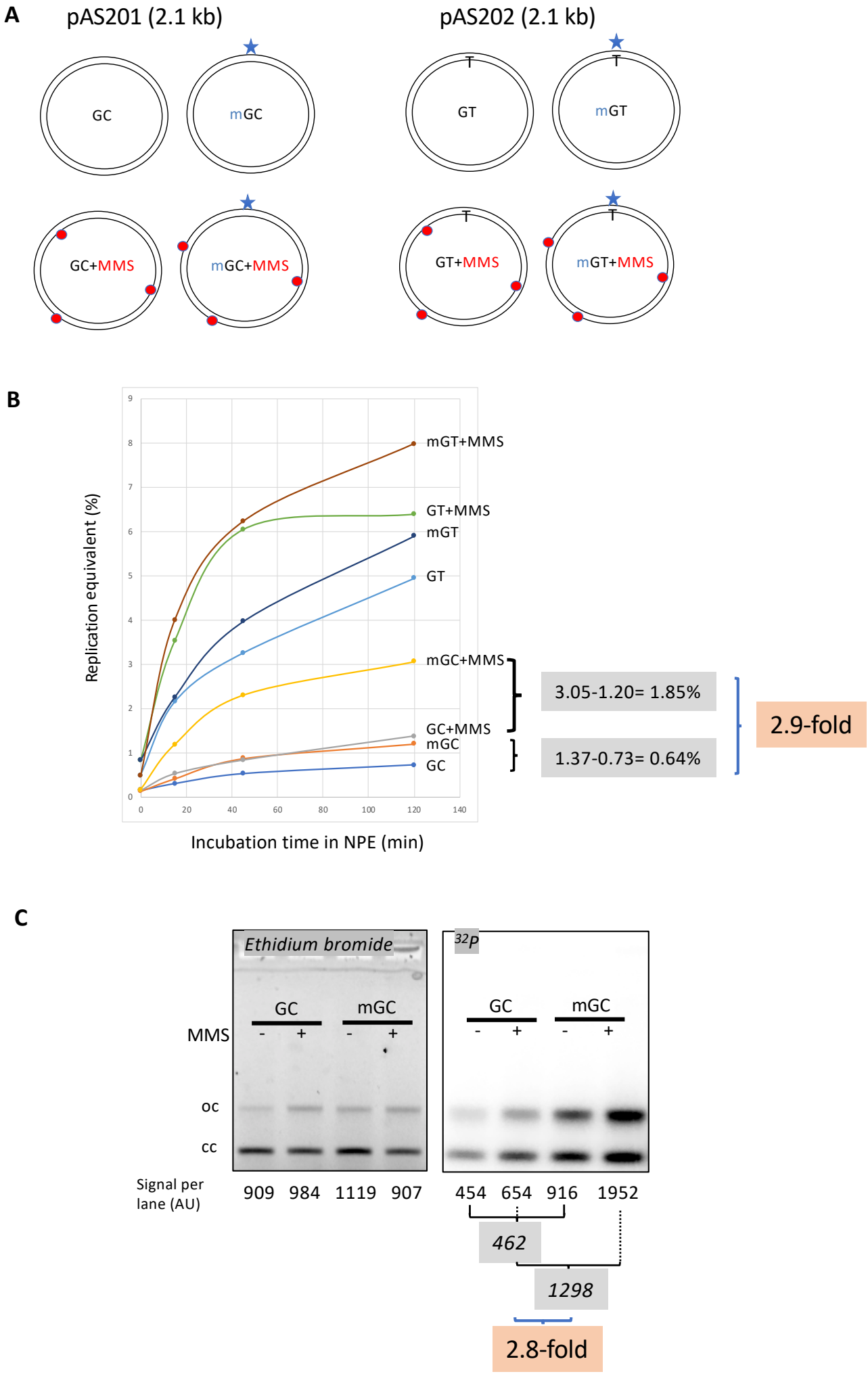
A
pAS201 (2.1 kb)
pAS202 (2.1 kb)
GC
mGC
GT
mGT
GC+MMS
mGC+MMS
GT+MMS
mGT+MMS
B
Replication equivalent (%)
Incubation time in NPE (min)
mGT+MMS
GT+MMS
mGT
GT
mGC+MMS
GC+MMS
mGC
GC
3.05-1.20= 1.85%
1.37-0.73= 0.64%
2.9-fold
C
Ethidium bromide
32P
GC
mGC
MMS
oc
cc
Signal per lane (AU)
909 984 1119 907
454 654 916 1952
462
1298
2.8-fold

Figure 3

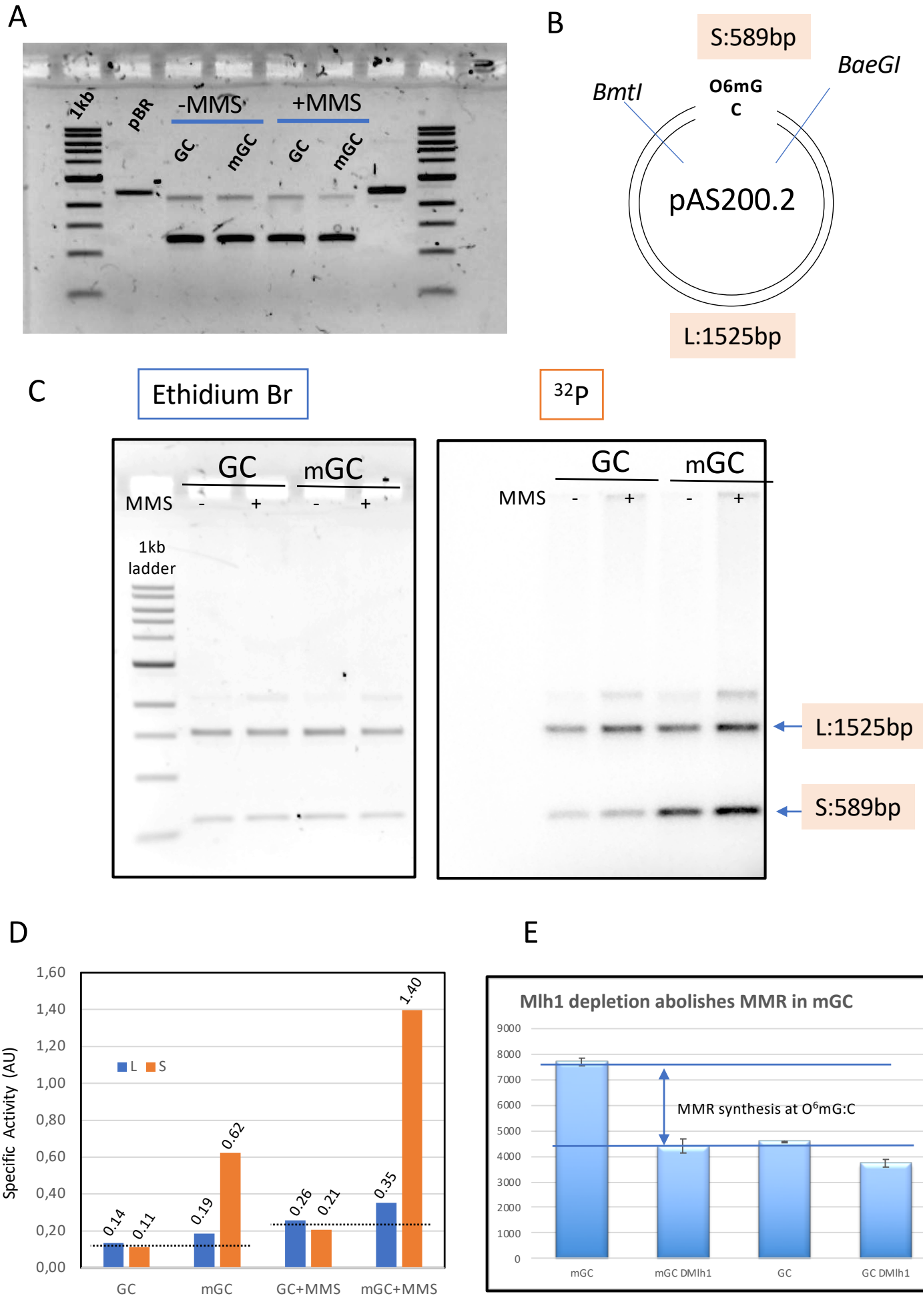


Figure 3-figure supplement 1

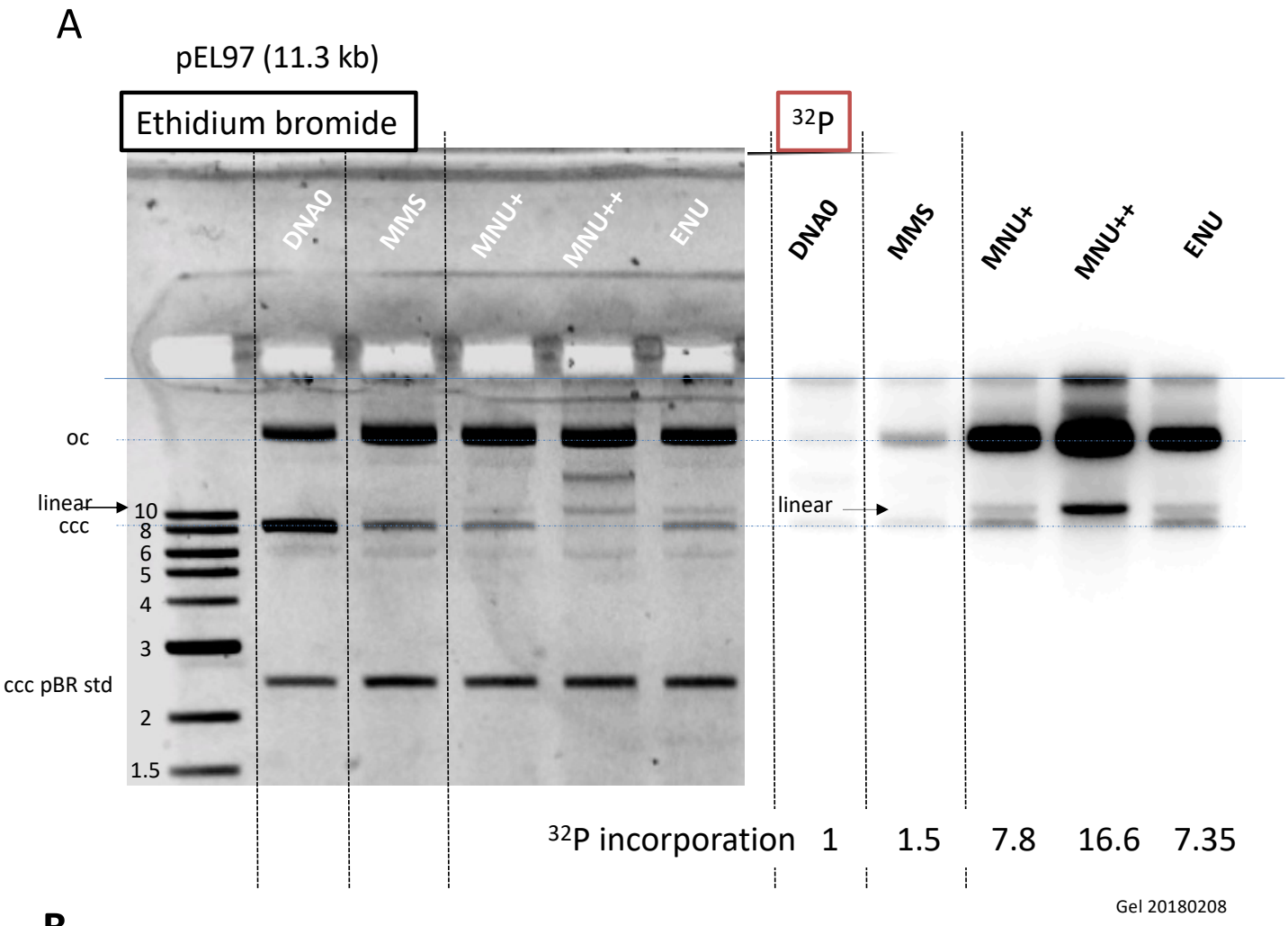
A
pEL97 (11.3 kb)
Ethidium bromide
32P
DNA0
MMS
MNU+
MNU++
ENU
oc
linear
ccc
10
8
6
5
4
3
ccc pBR std
2
1.5
linear
32P incorporation 1 1.5 7.8 16.6 7.35
Gel 20180208

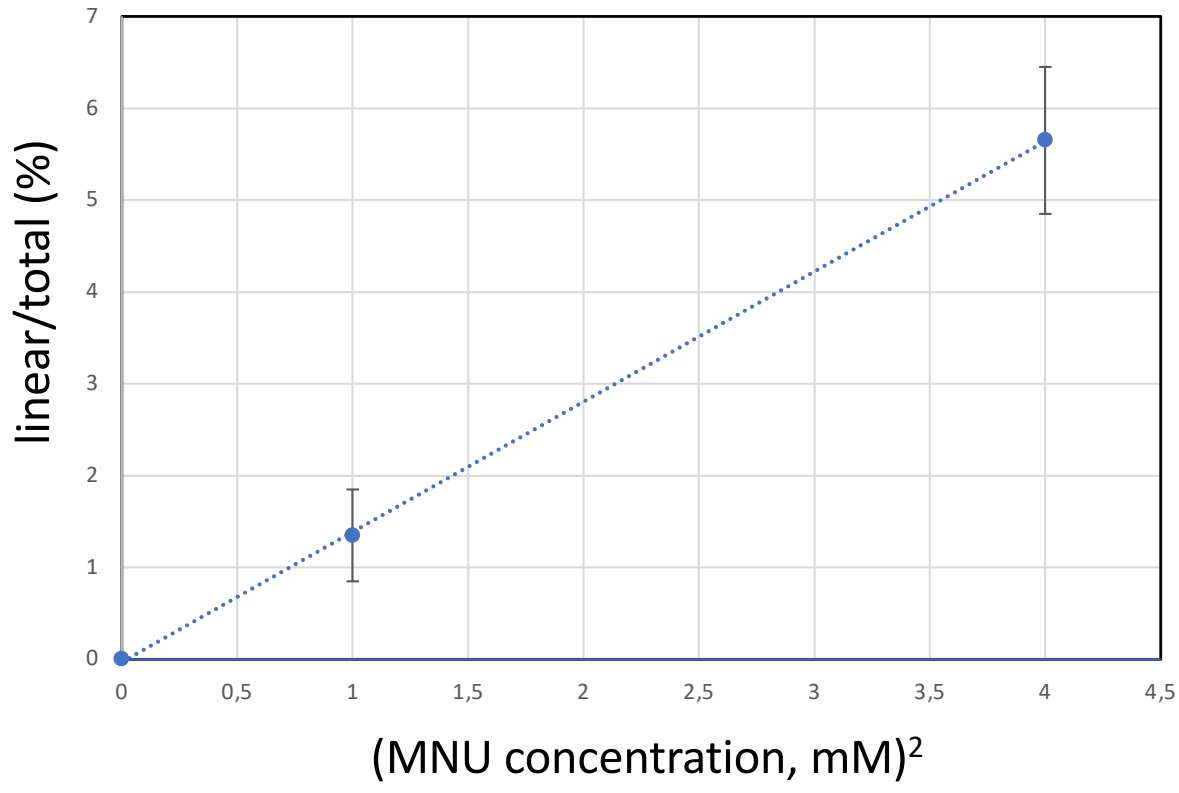
B
linear/total (%)
0
1
2
3
4
5
6
7
0
0,5
1
1,5
2
2,5
3
3,5
4
4,5
(MNU concentration, mM)2

Figure 4

pEL97 (11.3 kb)

A

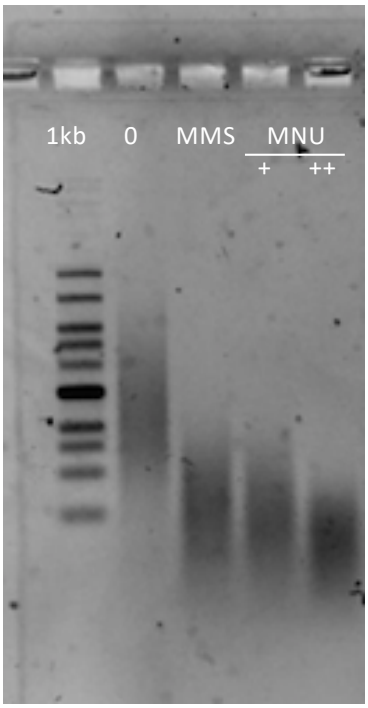


B

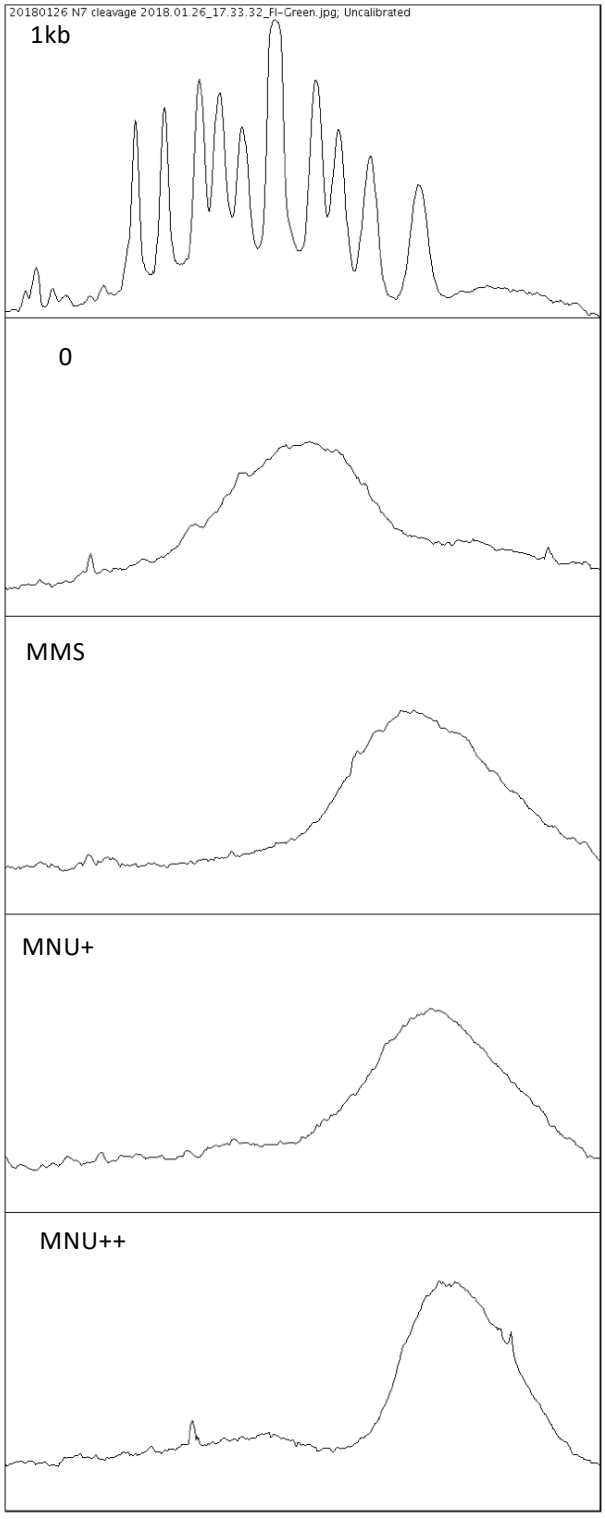


C

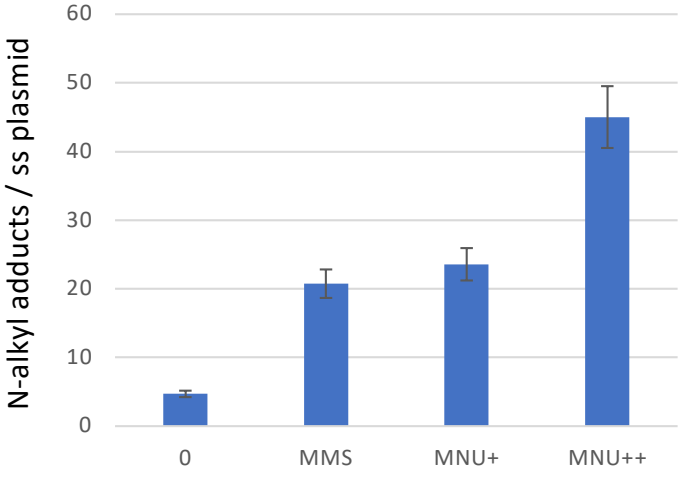


Figure 4-figure supplement 1

pEL97 (11.3 kb)

A

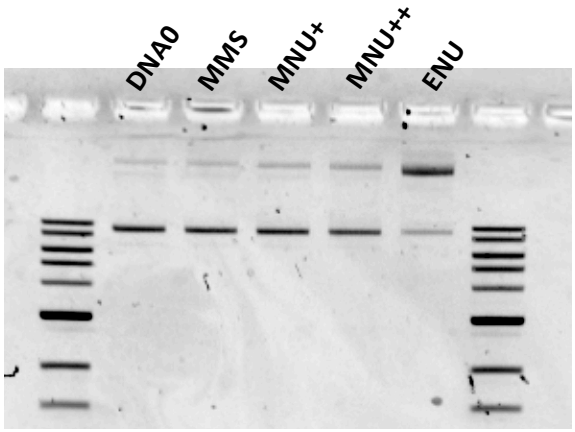


B

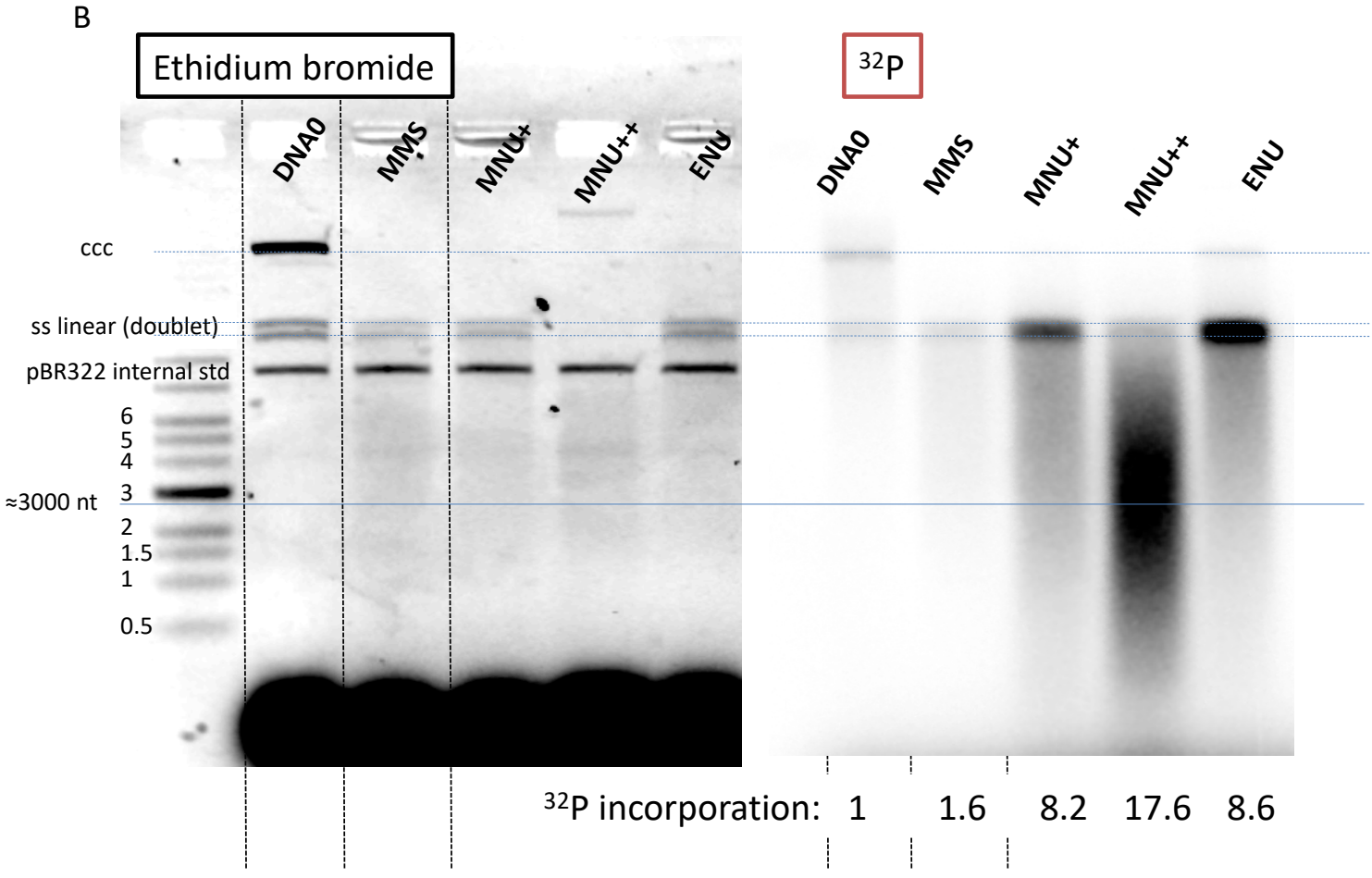


Figure 4-figure supplement 2

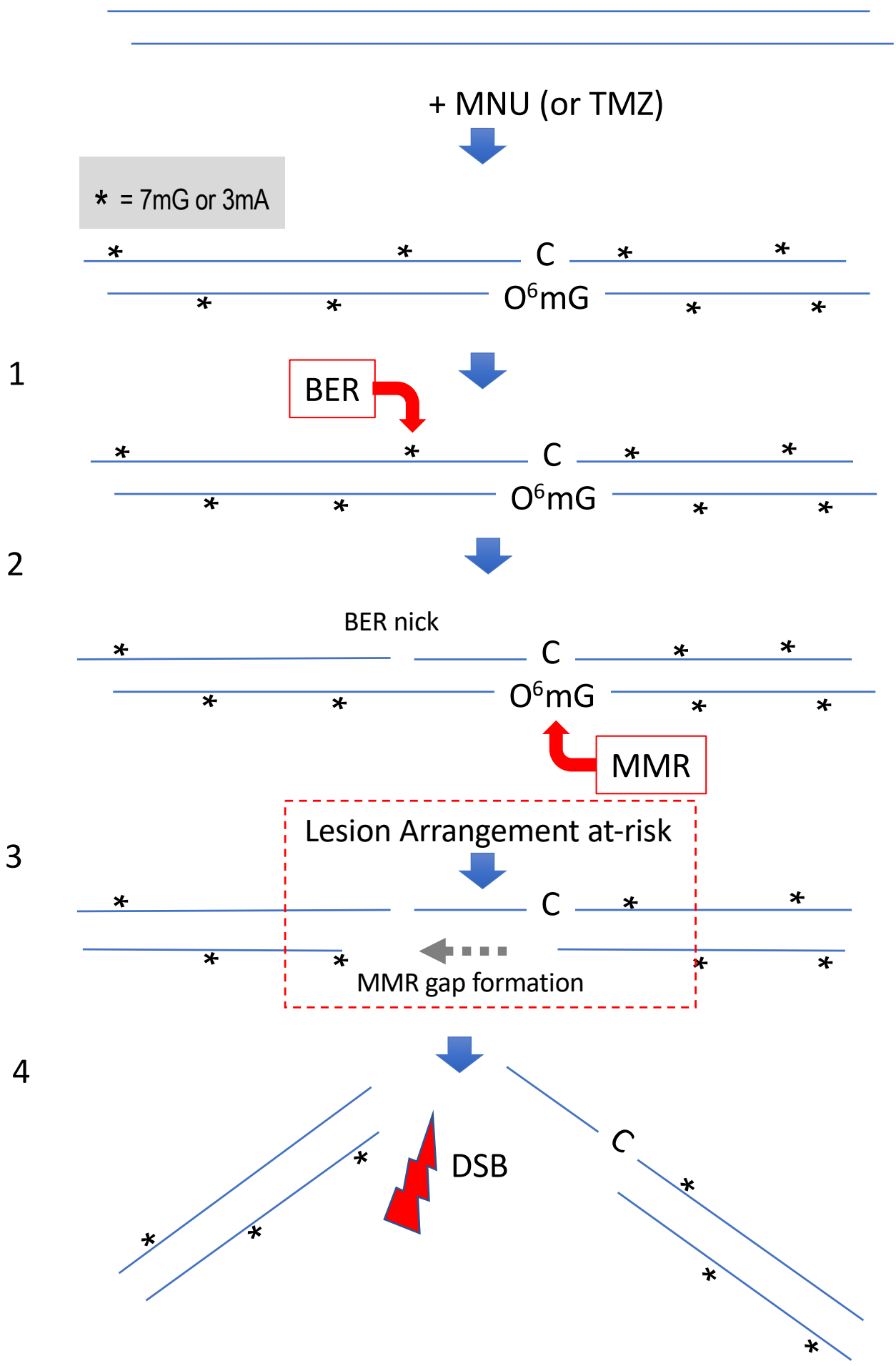
+ MNU (or TMZ)
* = 7mG or 3mA
C
O6mG
1
BER
2
BER nick
MMR
3
Lesion Arrangement at-risk
MMR gap formation
4
DSB

Figure 5